

# MEASUREMENTS OF PARTICLE COLLISION PROPERTIES

A Thesis

Presented to the Faculty of the Graduate School  
of Cornell University

in Partial Fulfillment of the Requirements for the Degree of  
Master of Science

by

Samuel F. Foerster

May 1993

© Samuel F. Foerster 1993

ALL RIGHTS RESERVED

## BIOGRAPHICAL SKETCH

Samuel F. Foerster was born the seventh of eight children on the twenty-third of December, 1969. Growing up in Pomona Park, Florida brought with it some of the joys of rural life- swimming in lakes without names, squirrel hunting, and bike riding from here to the convenience store at the end of the universe. Crescent City High School was the typical surreal experience, involving expensive sneakers, Friday night football games, track meets, after-school practices, parking at the drive-in, and friends who swore their undying devotion to one another. Campus life at Stetson University proved more focused, though the experience involved a number of frat parties, two near misses, and three spring breaks in Panama City. After receiving a B.S. in Physics, Sam went on to Cornell University, where he contributed to several experimental projects in the field of granular flow. Upon completing his M.S. in mechanical engineering, he began work as an associate engineer with Florida Power & Light, where he gained experience in design and project engineering at combined cycle power plants.

## ACKNOWLEDGMENTS

This work was supported by the Pittsburgh Energy Technology Center of the U.S. Department of Energy under the Granular Flow Advanced Research Objective through contract DE-AC22-91PC90183. The author is indebted to Hongder Chang, who participated in the conception of the apparatus, built a prototype, and designed the control electronics. He is equally grateful to Khedidja Alia, who identified the principal difficulties in running the experiments. He wishes to thank James Jenkins and Otis Walton for stimulating discussions in the course of the project, Cedriane DeBoucaud for sharing her photographic expertise, and Edward Jordan, Mark Tuccio, and Adam Lorenz for helping with the experiments. The acetate and glass spheres were donated by Thomas G. Drake and Winsted Precision Ball Co., respectively. Special thanks are extended to my advisor, Michel Louge, for his unfailing confidence and support.

## TABLE OF CONTENTS

List of Tables .....	vi
List of Figures .....	vii
List of Symbols .....	viii
Chapter 1: Introduction.....	1
Chapter 2: Binary Collisions.....	3
Chapter 3: Flat Plate Impacts.....	10
Chapter 4: Methods .....	13
I Overview .....	13
II Equipment.....	17
III Experimental Procedure.....	24
Chapter 5: Results .....	46
Chapter 6: Conclusions.....	52
Appendix A: Material Properties .....	54
Appendix B: Procedures .....	55
Alignment of Release Mechanisms.....	55
Determining Response Times, Pulse Widths & Shutter Speed.....	57
Photographing Binary Collisions.....	65
Appendix C: List of Manufacturers .....	76
References .....	77

## LIST OF TABLES

Table 1	Material properties .....	24
Table 2	Recommended development times for Press Maxx developer.....	33
Table 3	Collision coefficients .....	46
Table 4	Chauvenet's criterion results .....	47

## LIST OF FIGURES

Figure 1	Unit vector definitions.....	4
Figure 2	Experimental facility- side view.....	14
Figure 3	Experimental facility- top view.....	15
Figure 4	Stroboscopic photograph.....	16
Figure 5	Flat plate assembly.....	16
Figure 6	Control circuitry wiring diagram .....	18
Figure 7	Timing control circuitry output.....	19
Figure 8	Clippard ETO-3-12 solenoid pneumatic valve.....	20
Figure 9	Determining T1 pulse width.....	27
Figure 10	Position definitions and collision plane angle.....	36
Figure 11	Binary collisions of 3mm glass spheres.....	49
Figure 12	Binary collisions of 6mm acetate spheres.....	49
Figure 13	Impact of 3mm glass spheres on aluminum plate .....	50
Figure 14	Impact of 6mm acetate spheres on aluminum plate.....	50

## LIST OF SYMBOLS

### Notation

$X'$	- post-collision value of quantity $X$
$X_x$	- horizontal component of vector quantity $\mathbf{X}$
$X_y$	- vertical component of vector quantity $\mathbf{X}$

### Coefficient derivations

$e$	- coefficient of normal restitution
$\beta_0$	- coefficient of tangential restitution
$\mu$	- coefficient of friction
$\bar{v}_1$	- dimensionless pre-collision tangential component of relative velocity of point of contact
$\bar{v}_2$	- dimensionless post-collision tangential component of relative velocity of point of contact
P1	- particle 1; particle suspended from higher release mechanism and released first by timing control circuitry
P2	- particle 2; particle suspended from lower release mechanism and released second by timing control circuitry
$\mathbf{c}_i$	- pre-collision velocity of particle $i$ center of mass
$\mathbf{g}_i$	- pre-collision velocity of particle $i$ point of contact
$\mathbf{g}_{12}$	- pre-collision relative velocity of point of contact
$\hat{\mathbf{i}}, \hat{\mathbf{j}}$	- orthogonal horizontal and downward vertical unit vectors, respectively, which span the collision plane
$\mathbf{J}$	- impulse imparted on P1 by P2
$\mathbf{H}$	- angular momentum
$\mathbf{n}$	- unit vector normal to the surface at the point of contact
$\mathbf{t}$	- unit vector tangent to the surface at the point of contact
$\bar{\omega}_i$	- angular velocity of particle $i$
$\bar{\omega}$	- collision orientation angle measured positive clockwise from $\mathbf{g}_{12}$ to $\mathbf{n}$
$I_{icm}$	- particle $i$ moment of inertia about center of mass
$m_i$	- mass of particle $i$
$r_i$	- radius of particle $i$
$\bar{d}_i$	- diameter of particle $i$

### Flat plate calculations

$a$	- sphere radius
$c$	- speed of shear waves in flat plate
$E_p$	- Young's modulus for flat plate material
$E_s$	- Young's modulus for sphere material
$\bar{\rho}_p$	- density of flat plate material
$\bar{\rho}_s$	- density of sphere material
$s_{crit}$	- critical distance from plate supports beyond which $e$ is no longer dependent
$T_c$	- Hertzian contact time for sphere impacting flat plate
$\nu_p$	- Poisson's ratio for flat plate material

$\nu$  - Poisson's ratio for sphere material

### Timing delay and shutter speed calculations

R1	- time interval separating T1 leading edge and trigger of camera shutter release
T1	- P1 release mechanism trigger pulse
T2	- P2 release mechanism trigger pulse
T2 <sub>min</sub>	- minimum value of T2 which still guarantees in-time release of P2
T2 <sub>max</sub>	- maximum value of T2 which still guarantees in-time retraction of second release mechanism
T3	- retraction mechanism trigger pulse
$s_{coll}$	- height of point of contact above drop stage at time of collision
$s_{fieldbottom}$	- vertical distance separating top of suspended P2 and bottom of camera field of view
$s_{fieldtop}$	- vertical distance separating bottom of suspended P2 and top of camera field of view
$s_i$	- vertical distance separating bottom of particle i and drop stage
$s_{P1to rel.mech.}$	- vertical distance separating bottom of suspended P1 and top of second release mechanism
$t_{cam.response}$	- delay observed between trigger of shutter release and opening of camera shutter
$t_{flighti}$	- expected time of flight between release of particle i and impact with drop stage
$t_{fullretract}$	- time interval separating T1 leading edge and full retraction of lower release mechanism
$t_{P1to rel.mech.}$	- time interval separating T1 leading edge and bottom of particle 1 at top of second release mechanism
$t_{P2to field}$	- time interval separating T1 leading edge and bottom of P2 at top of camera field of view
$t_{responsei}$	- average time interval separating leading edge of trigger pulse and actual release of particle i (i=1,2) or full retraction of lower release mechanism (i=3)
$t_{responseimin}$	- minimum observed interval separating leading edge of trigger pulse and actual release of particle i (i=1,2) or full retraction of lower release mechanism (i=3)
$t_{responseimax}$	- maximum observed interval separating leading edge of trigger pulse and actual release of particle i (i=1,2) or full retraction of lower release mechanism (i=3)
$t_{shutter}$	- time span during which particles are in the camera field of view
$t_{T1tocoll}$	- time interval separating leading edge of T1 and bottom of particle 1 at $s_{coll}$
$t_{T2tocoll}$	- time interval separating leading edge of T2 and top of particle 2 at $s_{coll}$
$\Delta y_{fieldofview}$	- vertical extent of field of view

### Data analysis

$\angle$  - angle separating plane of focus and collision plane

$c_{iyposj}$	- vertical velocity component of particle i center of mass at position j
$g$	- acceleration due to gravity
$strobehz$	- frequency of strobes in cycles per second
$\Delta t$	- period between strobe flashes
$t_{coll}$	- time required for particles to travel from position 1 to collision, calculated from pre-collision trajectories
$t_{collpost}$	- time required for particles to travel from collision to position 2, calculated using post-collision trajectories
$x_{ij}, y_{ij}$	- coordinates of particle i center of mass at position j
$x_i(t), y_i(t)$	- coordinates of particle i center of mass as functions of time
$x_{icoll}, y_{icoll}$	- coordinates of particle i center of mass at collision, calculated using post-collision trajectories

## ABSTRACT

Spherical particles in binary collisions and impacts with flat plates are studied. Pre- and post-impact relative velocities of the points of contact are assumed to be uniquely related through the coefficients of normal restitution, tangential restitution and friction, defined, respectively, as

$$\mathbf{g}_2 \cdot \mathbf{n} = e(\mathbf{g}_{12} \cdot \mathbf{n})$$

$$\mathbf{g}_2 \cdot \mathbf{t} = \beta_0(\mathbf{g}_{12} \cdot \mathbf{t})$$

$$|\mathbf{J} \cdot \mathbf{t}| = \mu(\mathbf{J} \cdot \mathbf{n})$$

where  $\mathbf{n}$  and  $\mathbf{t}$  are the unit normal and unit tangent vectors,  $\mathbf{g}_{12}$  and  $\mathbf{g}_2$  are the pre- and post-impact relative velocities of the points of contact, and  $\mathbf{J}$  is the impulse imparted on the first particle by the second. Collisions are assumed to be of two types, differentiated by the behavior of the point of contact at the time of collision. If the point of contact locks during a collision, the collision is said to be one of sticking contact, and  $\beta_0$  is assumed to be meaningful. If the point of contact slips during the collision, the impact is said to be one of sliding contact, and the normal and tangential components of the impulse are assumed to be related through  $\mu$ .

A facility is designed to release two spherical particles such that the particles collide with no initial angular velocity or horizontal component of translational velocity of the center of mass. Collision orientation and pre-and post-collision translational velocities are recorded. The observed values are used to calculate the dimensionless tangential components of pre- and post-collision relative velocities:

$$\beta_1 = \frac{\mathbf{g}_{12} \cdot \mathbf{t}}{\mathbf{g}_{12} \cdot \mathbf{n}}$$

$$\beta_2 = \frac{\mathbf{g}_2 \cdot \mathbf{t}}{\mathbf{g}_{12} \cdot \mathbf{n}}$$

A plot of  $\bar{v}_2$  versus  $\bar{v}_1$  yields two linear regimes corresponding to sticking and sliding contact. Coefficients appropriate to each regime are then calculated for each data point and averaged. Results are presented for 3mm glass and 6mm acetate spheres.

A modified form of the same facility is used to drop a single spherical particle with no spin onto a thick aluminum plate. Plate inclination and pre- and post-impact translational velocities are measured for several collisions. The information is used to calculate the coefficients appropriate to each regime observed in the plot of  $\bar{v}_2$  versus  $\bar{v}_1$ . Results are presented for 3mm glass and 6mm acetate spheres.

## CHAPTER 1: INTRODUCTION

Granular flows may be observed in a diverse number of industrial and environmental settings- pulverized coal power plants, snow covered mountains, beaches, grain elevators, rock quarries, pharmaceutical manufacturing facilities. Though an important class of material flows, the relationships between individual particle properties and even the most global attributes of a granular flow are not yet well understood. Given a set of non-ideal particles and boundary conditions, it is not generally possible to predict velocity profiles and solid volume fraction distributions. Theoreticians in the field are currently working to develop a kinetic theory for flows of solid particles that calculates the concentration, velocity and velocity fluctuations in terms of empirically determined material constants and boundary conditions. The particle agitation is characterized by the "granular temperature", which is proportional to the root mean square velocity fluctuations of the grains. The empirical constants, defined as the coefficients of normal restitution, tangential restitution and friction, uniquely relate the pre- and post-collision relative velocities of the points of contact for both binary inter-particle and particle-boundary impacts. Theoretical results for ideal particle geometries and boundary conditions have compared favorably with computer simulation results presented by Walton (1988), shear cell experiments conducted by Craig, Buckholz, and Domoto (1986), and chute flows studied by Johnson, Nott, and Jackson (1990).

The purpose of the present research is to develop a mechanism by which the coefficients of normal restitution, tangential restitution and friction may be calculated for particles interacting in a binary collision. Results will be reported for 3mm glass and 6mm cellulose acetate spherical particles. Also, a means will be developed for measuring the collision coefficients of a particle rebounding

from an inclined flat plate. Results will be given for 3mm glass and 6mm cellulose acetate spheres impacting a thick aluminum plate.

## CHAPTER 4: METHODS

### I Overview

The coefficients of restitution and friction for a particular collision may be calculated if the collision orientation and relative pre- and post-collision velocities are known. In general, the relative velocities of the point of contact of two rigid bodies include angular velocity terms which are difficult to quantify experimentally. However, conservation of angular momentum about the point of contact allows expression of the post-collision angular velocities in terms of particle masses, translational velocities and pre-collision spin. Thus, if two bodies are made to collide without initial spin, the collision may be fully described by the knowledge of pre- and post-collision translational velocities, masses, and collision orientation.

Our binary collision facility is designed to release two spherical particles in such a fashion as to collide with zero pre-collision spin in repeatable relative orientations and translational positions. The particles are suspended by maintaining partial vacuum across very small orifices with which the particles are in contact. The upper release mechanism is mounted on a two degree of freedom carriage, making vertical alignment with the lower release mechanism possible. This lower mechanism is mounted to a solenoid through a one-dimensional sliding bearing, allowing retraction upon release of the second particle. The particles are released by tripping a three way solenoid valve placed in the line connecting the contact orifice to the vacuum pump. When energized, the solenoid opens directly to atmosphere while simultaneously closing the vacuum line. Engagement of the solenoid valves, retraction of the lower release mechanism, and release of the camera shutter are coordinated

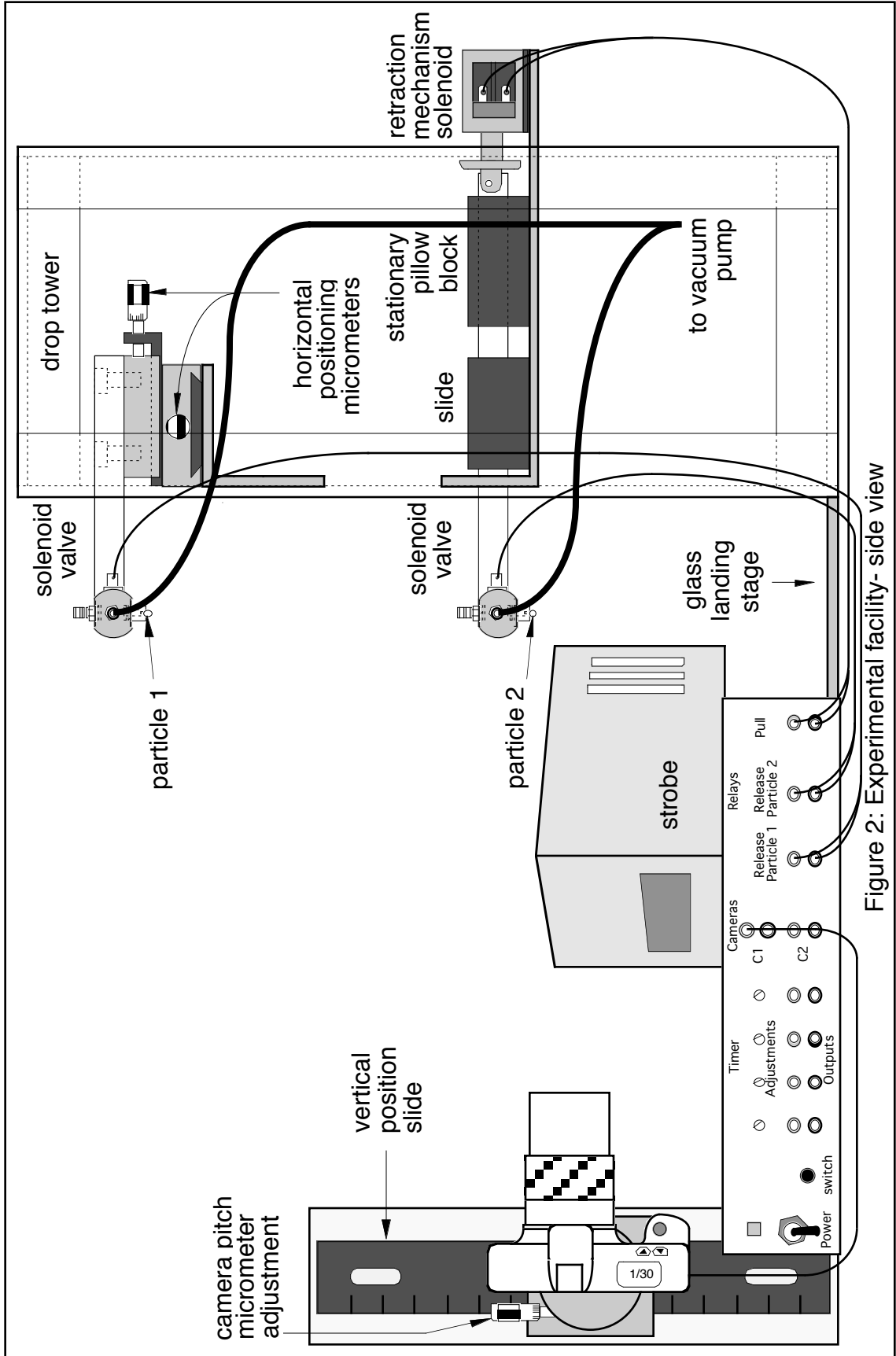


Figure 2: Experimental facility- side view

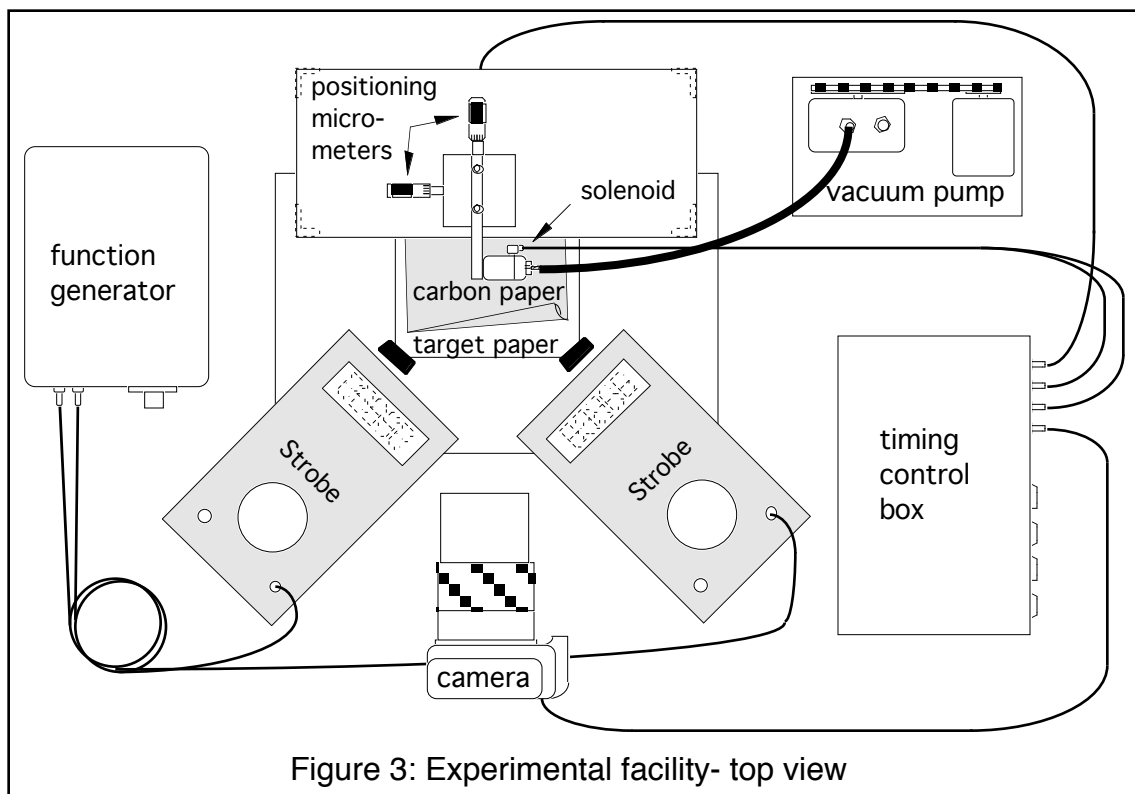


Figure 3: Experimental facility- top view

using a set of timing circuits. By adjusting the time interval separating the two releases, the collision is made to occur in the field of view of the camera. Two synchronized, symmetrically arranged Shimpo DT-301 digital strobes provide the only lighting, so each photograph is an accurate record of the positions of the particles as functions of time (Figure 4). The landing positions of the two particles are recorded and used to determine the angle formed by the intersection of the photo plane and the plane of the particle trajectories, allowing the projected positions observed in the photo to be corrected. The ballistics of the particles are then analyzed to determine the collision orientation as well as the pre- and post-collision translational velocities of the centers of mass. Finally, these values are substituted into the expressions developed in the section "Binary Collisions", yielding  $e$ ,  $\beta_0$ , and  $\mu$ .

The same facility is used to conduct the flat plate experiments. A flat aluminum plate is mounted directly beneath the release mechanisms on a

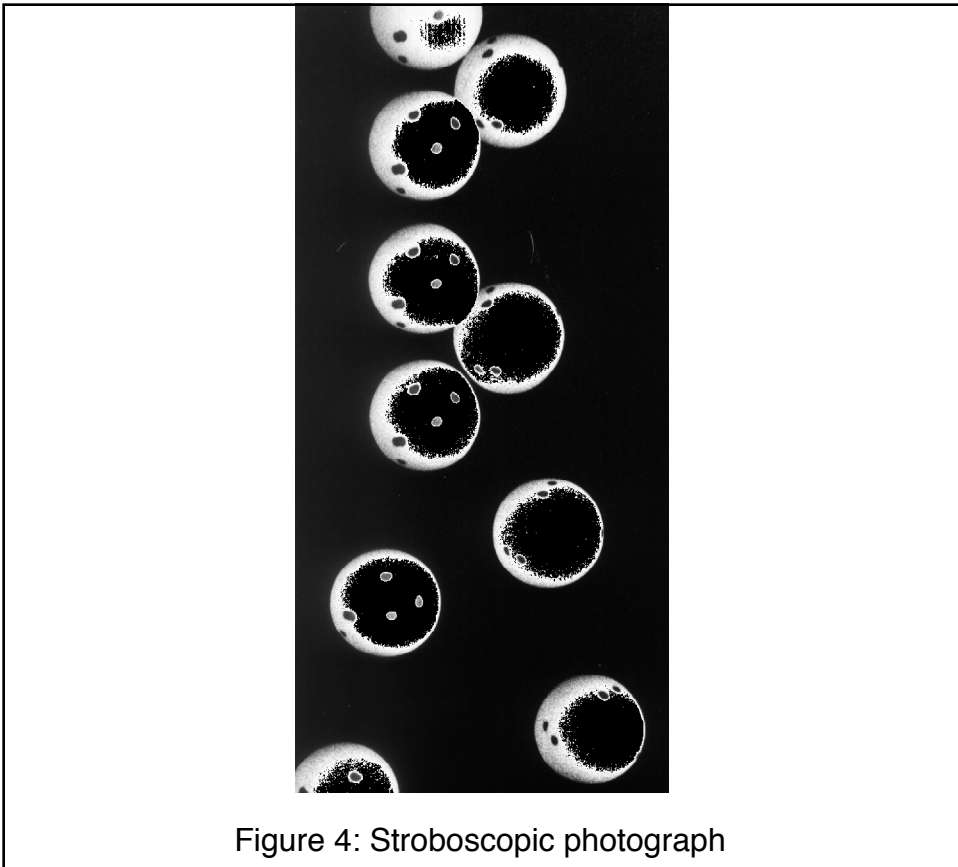
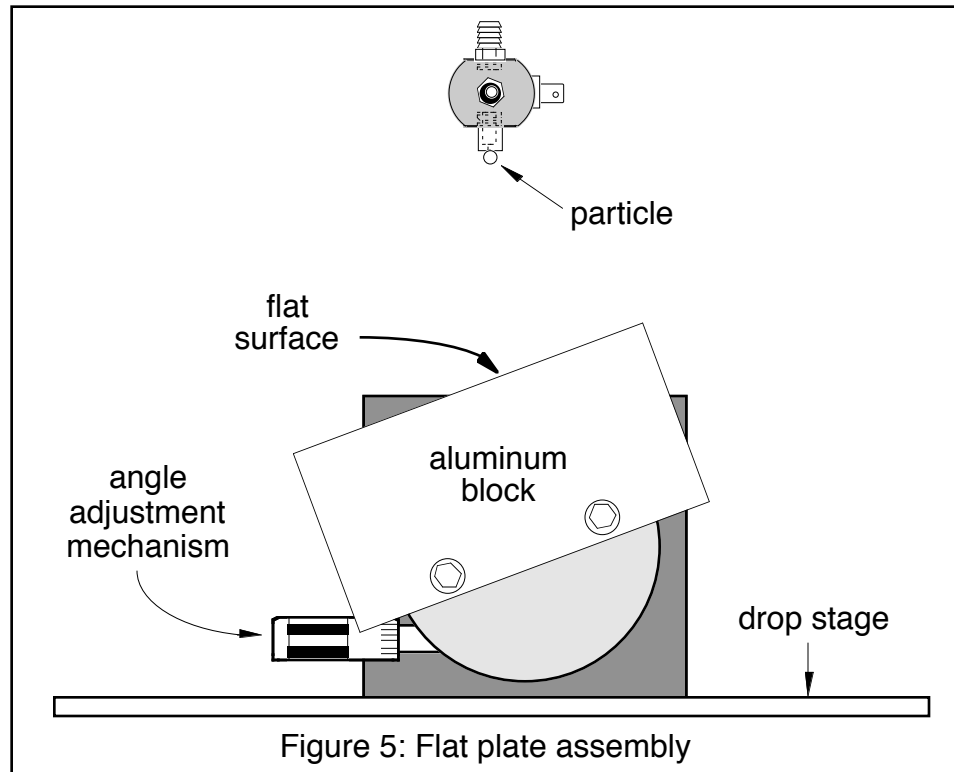


Figure 4: Stroboscopic photograph



rotating table whose axis of rotation is parallel to the camera line of focus (Figure 5). The camera position is adjusted so that the plate is in the bottom of the field of view, and the timing circuits are set to open the camera shutter when the particle reaches the top of the field of view. Again, synchronized strobes are the sole sources of illumination, so photographs provide all the information needed to calculate the pre- and post-impact particle velocities. These velocities are then used in the expressions developed in the section "Impacts Between Spherical Particles and Flat Plates" to determine the values of the coefficients of normal restitution, tangential restitution and friction.

## II Equipment

### A. Timing Control Circuitry

At the heart of the experiment is a set of timing circuits used to coordinate the release of the particles, retraction of the second release mechanism, and opening of the camera shutter. The circuitry includes two DC power supplies, AC and DC solid state relays, a bounceless activation switch, "one-shot" pulse generators, invertors, type 555 timers, and adjustable potentiometers.

One power supply provides the 5VDC for the logic/control circuitry. The control sequence is initiated by pressing a push-button switch, which sends a clean inverted initial pulse to a "one-shot" circuit designed to provide an output pulse of the order of hundreds of microseconds. This output is first channeled through an invertor, then used to trip two independent 555 timing circuits, designated T1 and R1, whose pulse widths are set using adjustable potentiometers. A relay controlling the electronic camera shutter is set to trip on the trailing edge of R1, while the output of the T1 timer serves to actuate a DC solid state relay controlling the pneumatic valve for particle one. The inverted

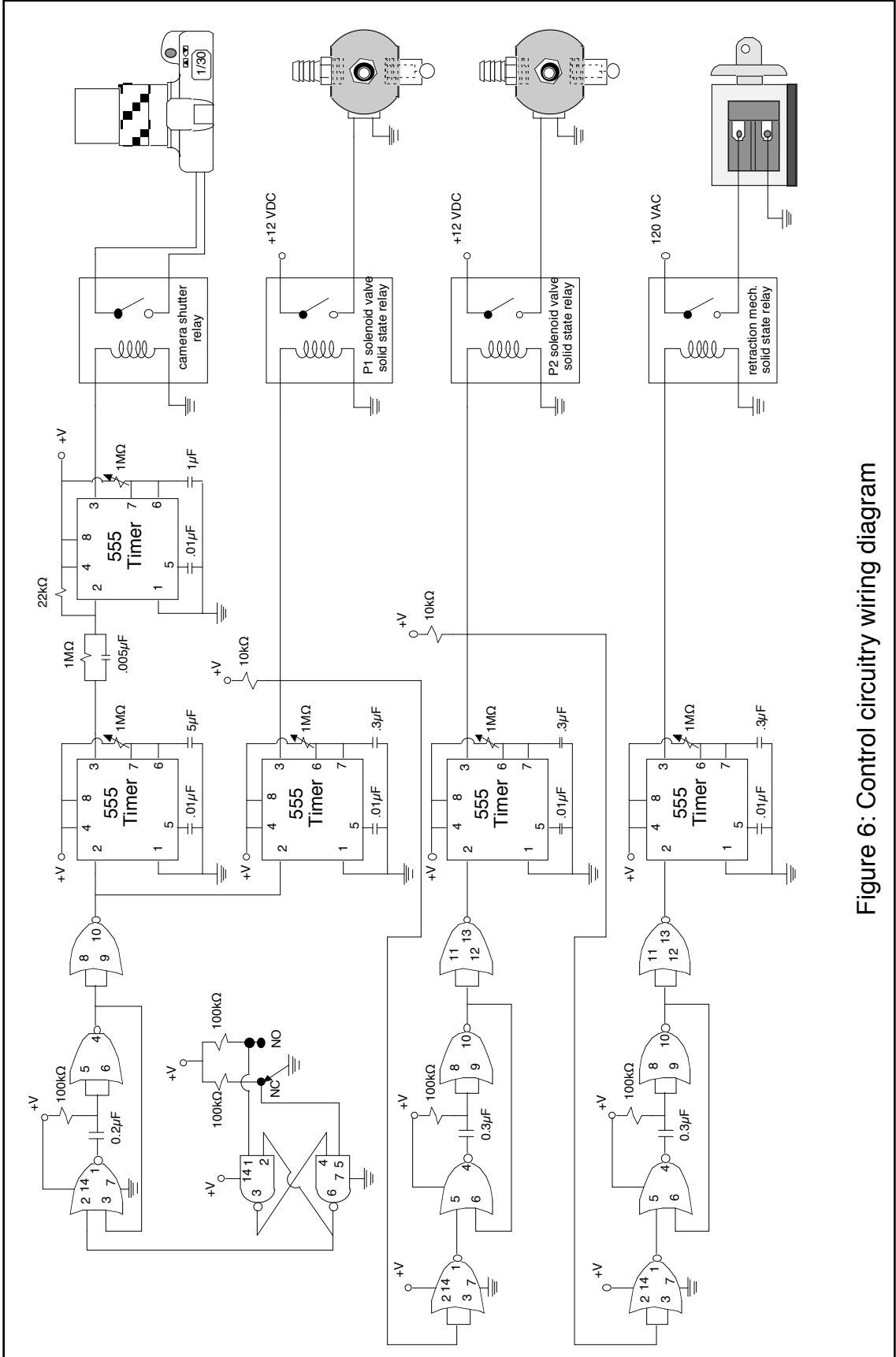
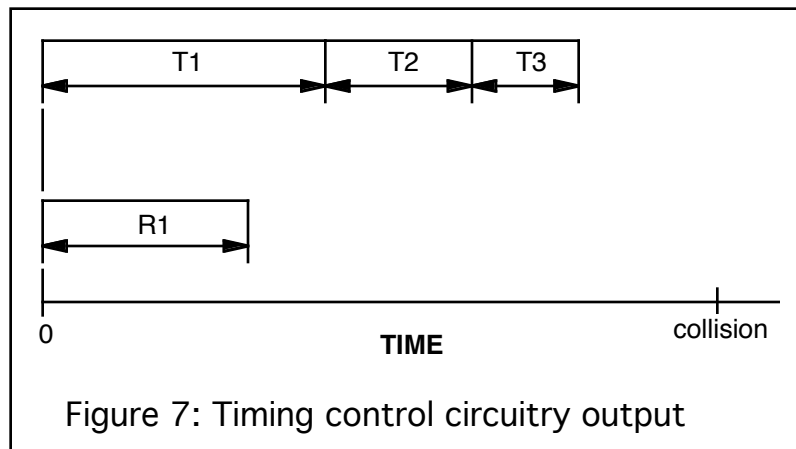


Figure 6: Control circuitry wiring diagram

T1 pulse also serves as the input to a second one-shot circuit whose inverted output is used to start a third 555 timer, designated T2. The adjustable output of this timer trips a second DC solid state relay which controls the pneumatic valve for particle two. Inverted, T2 also serves as the input for a third one-shot circuit whose inverted output is used to initiate the fourth and final 555 timer, designated as T3. The output of T3 closes the AC solid state relay controlling the retraction solenoid. The complete wiring diagram is given in Figure 6, while the simple relationships between the control circuitry output pulses are shown in Figure 7.

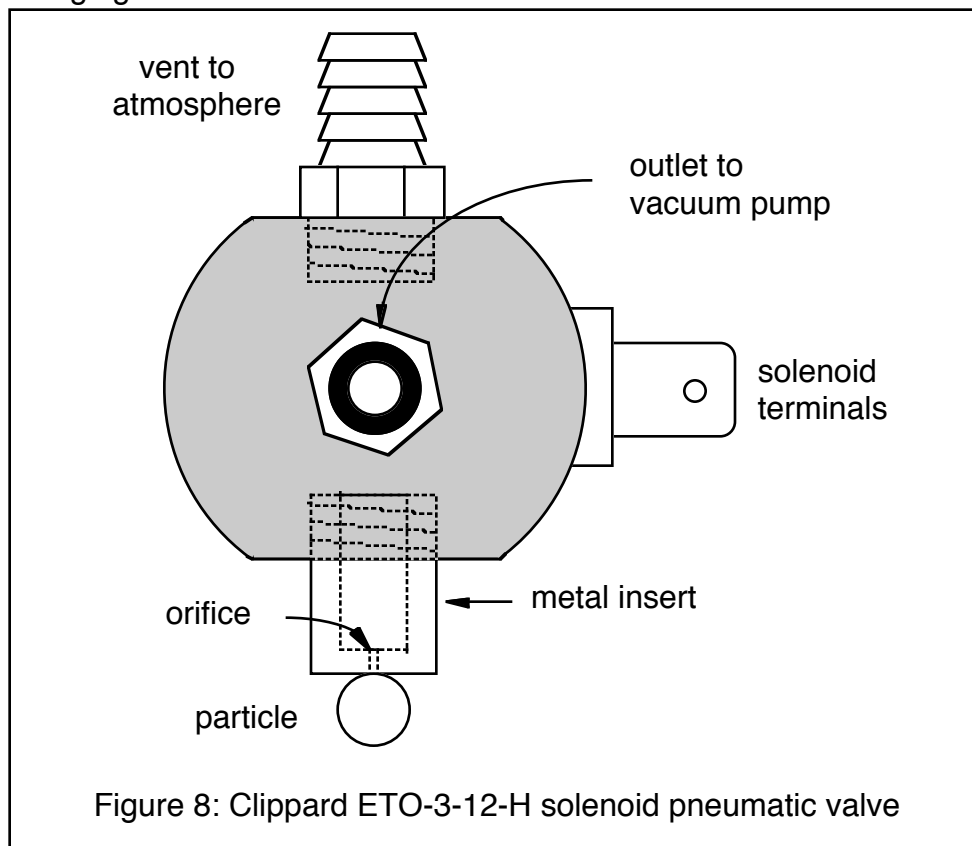


## B. Release Mechanisms

Each release mechanism is designed to yield excellent spatial and temporal reproducibility while imparting no angular velocity in the spherical particle it releases. The particle is suspended from a small circular orifice across which a partial vacuum is drawn. When the Clippard ETO-3-12 solenoid pneumatic valve in line between the orifice and the vacuum pump is tripped, the vacuum is broken and the particle is released. The spatial variance in landing positions, as well as the moments applied to the spherical particle through the mechanism during release, is minimized by maximizing the ratio of particle

diameter to orifice diameter. In our current configuration, ten consecutive releases of a 3mm glass particle from an orifice of .38mm positioned at a height of .6m produce a locus of landing positions 1.5mm in diameter. Temporal consistency of the mechanism, which appears related to the surface properties at the orifice, is maximized when a non-beveled orifice is drilled into a polished metal surface.

Other points of interest regarding release mechanism design are the choice and placement of the solenoid valves. Direct current solenoid valves are used in order to avoid the variance in response times associated with the cyclic nature of alternating current. Each valve is positioned such that the particle can be suspended from a short insert threaded directly into the valve port, as seen in the following figure:



Although this configuration fails to isolate mechanically the valve from the particle, it minimizes the distance between the vacuum breaker and the orifice

with which the particle is in contact. Since the moving part in the Clippard pneumatic valve has a small moment of inertia, direct mechanical contact between the valve and the particle has no observable effect on the spatial reproducibility of the mechanism. However, minimizing the distance between the orifice and the vacuum breaker, along with maximizing the pressure differential across the orifice, reduces the time required for pressure at the orifice to equilibrate after the valve is activated. This, in turn, reduces the amount of delay time required between tripping the second solenoid valve and activating the retraction mechanism.

### C. Drop Stage

Carbon paper is used to record the particle landing positions directly. First, a sheet of abylene tracing paper is taped securely to the glass plate lying flat in the drop zone of the particles. Carbon paper is placed over the abylene, and the impact points of the particles are recorded as small dark dots on the tracing paper.

In developing this method of recording the landing positions, several observations were made. Since the amount of pigment transferred from the carbon paper to the white paper is a function of the normal impulse imparted on the particle by the landing stage, it is important to maximize the elasticity of the impact between the particle and the stage. This suggests that a smooth, hard material be used to back a sheet of thin, dense white paper. Also, the carbon paper must be positioned so that no air bubbles exist at the interface with the white paper. We found that the impact positions of glass beads as small as two millimeters can be recorded when abylene tracing paper is used with standard carbon paper and a plate glass stage.

#### D. Photographic Setup

Photographic equipment includes an electronically triggered Minolta 5000i body with a 90mm Tamron telephoto lens, two Shimpo DT-301 portable digital stroboscopes, a function generator, 3200 ASA Kodak Tmax black and white film, and a black felt background. The camera is oriented for portrait style photographs on a fully adjustable mount. The distance of the camera from the collision plane is dictated by the minimum focal length of the lens. The strobes are positioned symmetrically about the camera and at right angles to one another. The black felt background is hung several feet from the camera lens.

The Minolta 5000i body is used because it can be triggered using an external, electronically controlled relay. This makes it possible to coordinate the shutter release with the release of the particles. The 90 mm telephoto lens offers an attractively sized field of view, approximately 8cmX6cm at an object distance of 24cm, without requiring a prohibitively large amount of light. The optimum size for the field of view is approximated by considering several factors: maximum strobe frequency, velocities of the particles while in the field of view, number of pre- and post-collision exposures required by the data analysis formulas, and the variance in the release times of the solenoid valves. The minimum required number of exposures multiplied by the minimum period between strobe flashes gives an estimate of the minimum time required in the field of view. Multiplying this time by the average velocity of the first particle while in the field of view yields an approximate minimum vertical dimension, which is then increased by a factor of the variance in release times multiplied by the average velocity.

The Shimpo strobes are chosen for their compact size, which permits easy positioning, and for their relatively low cost. The choice to use two strobes fired simultaneously offers some important advantages. First, twice as much

light is shed on the particles as would be possible with only one strobe. This allows for an increase in the lens aperture setting and, therefore, the depth of field, improving the odds of the particles remaining in focus even when alpha, the angle separating the collision and photo planes, is relatively large. Second, the strobes can be symmetrically placed about the camera, providing more even illumination of the sphere surfaces. Since a CAD (Computer Aided Design) program is eventually used to determine the positions of the particle centers from the extents of the particle perimeters, complete illumination of the spheres is important.

Though the illumination provided by the strobes is intense, the pulses are necessarily very short- approximately  $25\mu\text{s}$ . Thus, it is still necessary to use high speed 3200 ASA film. This type of film produces a noticeably more grainy negative than less sensitive varieties, but the distinction proves to be an entirely aesthetic one. Prior to analysis, the photos are scanned into PICT files at a resolution of 300DPI, a much lower resolution than that observed in the enlargements of the high speed negatives.

The combination of high speed film and one eighth second shutter times requires that measures be taken to prevent flooding of the film by stray light. Critical strobe vents are taped over, and black felt is placed over the drop tower and the background wall.

#### E. Flat Plate

The flat aluminum plate is mounted on a rotating table such that the normal to the plate surface is perpendicular to the axis of rotation, as shown in figure 5. The rotating table is then positioned so that the axis of rotation is both horizontal and parallel to the line of focus of the camera. The plate inclination is adjusted by turning the table to the desired position and locking.

In order to avoid the effect observed by Sondergaard, Chaney and Brennen (1990), the plate is manufactured and positioned so that the distance between the point of impact and the plate support is no less than the distance given by

$$s_{crit} = 1.57a \sqrt{\frac{E_p}{\rho_p}} \left[ (1 - v_s^2) + (1 - v_p^2) E_s / E_p \right]^{2/5} \left( \frac{\rho_s}{E_s} \right)^{2/5} (c_{1y} \cos \theta)^{1/5}$$

The material properties of interest are given below:

Table 1: Material Properties

	$E (Pa)$	$\nu$	$\rho (kg/m^3)$
Acetate	$3.2 \times 10^9$	.28	1300
Aluminum	$6.9 \times 10^{10}$	.33	2700
Glass	$7 \times 10^{10}$	.24	2500

In the case of an aluminum plate, a normal impact velocity of 2 m/s and a 3mm glass sphere,  $s_{crit}$  is equal to 1.4cm. For the case of a 6mm acetate sphere,  $s_{crit}$  increases to 5.7cm.

### III Experimental Procedure

#### A. Preparations

##### 1. Binary Collisions

Several requirements must be met if a binary collision is to be recorded on film:

- 1) the particles must collide in the field of view of the camera;
- 2) the camera must be in focus;

3) the camera shutter must be open when the particles are in the field of view;

4) the lens aperture must be at the correct setting.

Contained within the first item are several secondary considerations:

- 1a- the positions of the suspended particles must be vertically aligned so that a collision is possible;
- 1b- the time delay between the releases of the two particles,  $T_1$ , must be set such that the collision occurs at the desired vertical position;
- 1c- the second release mechanism must be retracted before the first particle collides with it. That is,  $T_2$  must be sufficiently large to allow the release of the second particle from the suspension mechanism, but it must be small enough to allow time for retraction of the release mechanism.

Each of these issues must be addressed before any data may be collected.

Ensuring that the suspended particles are aligned properly is one of the easiest requirements to meet. A sheet of abylene paper is taped to the glass stage in the drop zone, and a sheet of carbon paper is placed smoothly over it. The second release mechanism is moved to its fully forward position, and a particle is suspended from it. The particle is then released from this position several times, and the distribution of landing positions is noted. The second mechanism is then retracted, and the particle is suspended from the first release mechanism. Again, the particle is released several times from this position, and the landing positions are noted. If corrections are required, the position of the first release mechanism is modified using the micrometer adjustments on the carriage, and the process described above is repeated.

Determining the appropriate time delay between the two releases is somewhat more complicated. First, we must learn the response times associated with each of the solenoid valves as well as the retraction mechanism. Then we measure the vertical positions of the suspended particles. Finally, we decide where we want the collision to occur, and we perform a few calculations.

The response times associated with the valves are determined using an oscilloscope and a microphone. One channel of the oscilloscope is connected to the input of the solid state relay controlling the valve of interest, and the other channel is connected to a microphone through a small amplifier. The microphone is placed on the drop stage near the drop zone. A particle is suspended from the valve, the oscilloscope is reset, and the timing circuitry is tripped. Using the signals stored in the scope, we determine the amount of time elapsed between the leading edge of the solid state relay trigger pulse and the initial sound of impact with the stage. This process is repeated several times in order to obtain an average value. The expected time of flight of the particle, given by

$$t_{flighti} = \sqrt{\frac{2s_i}{g}}$$

where  $s_i$  is the vertical distance between the bottom of particle  $i$  and the drop stage, is then subtracted from the average release time to obtain the average response time for the mechanism. The response time for the retraction solenoid is calculated in very much the same way, except that the first channel of the oscilloscope is placed on the inputs for the AC solid state relay controlling the solenoid, and the microphone is placed near the retraction mechanism. The interval measured is that between the leading edge of the SSR trigger pulse and the sound of the retraction mechanism slamming to the fully retracted position.

With these equipment constants in hand, it is then a trivial matter to calculate the time interval required between the releases of the two particles. If we assume a head-on collision and we let  $s_{coll}$  be the height of the point of contact above the stage at the time of the collision, then the time interval separating the leading edge T1 and particle 1 at  $s_{coll}$  is given by

$$t_{T1tocoll} = t_{respons1} + \sqrt{\frac{2(s_1 - s_{coll})}{g}}$$

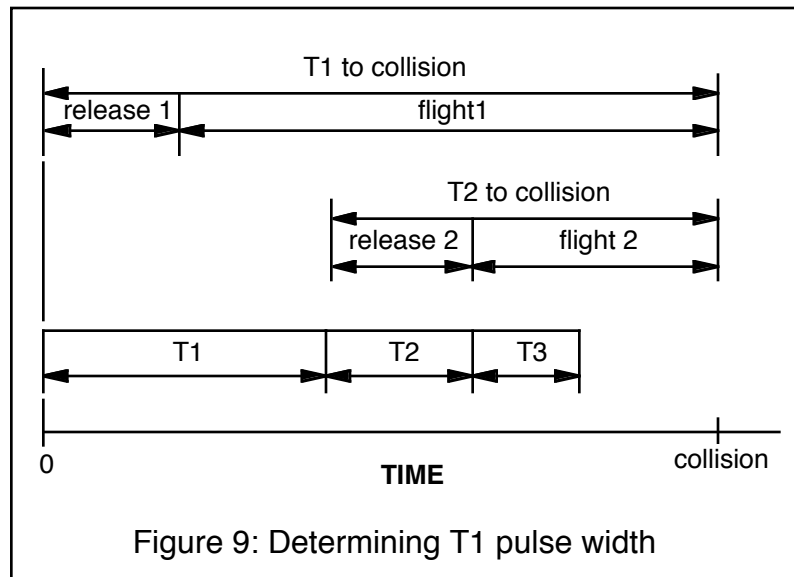
The corresponding interval for particle 2 is given by

$$t_{T2tocoll} = t_{respons2} + \sqrt{\frac{2(s_2 - s_{coll} + \Delta_2)}{g}}$$

and the time interval between the leading edge of T1 and the leading edge of T2, or the pulse width of T1, is given by

$$T1 = t_{T1tocoll} - t_{T2tocoll}$$

These calculations are summarized in the following graph:



The above value for T1 is then used to calculate the maximum allowable value for T2, the time interval between triggering the second solenoid valve and actuating the retraction mechanism. We know retraction must be completed by

the time the first particle reaches the vertical position of the second release mechanism. The first particle will reach this elevation in an amount of time no less than

$$t_{P1to2rel.mech.} = t_{response\ min} + \sqrt{\frac{2S_{P1to2rel.mech.}}{g}}$$

where  $t_{response\ min}$  is the minimum observed response time for the first solenoid valve and the second term on the right hand side is the time of flight of the particle from position 1 to the top of the second release mechanism. The second release mechanism will be fully retracted in an amount of time no more than,

$$t_{fullretract} = T1 + T2 + t_{response\ max}$$

where  $t_{response\ max}$  is the maximum interval observed between the leading edge of the AC SSR trigger pulse and full retraction. Thus, the maximum value for T2 which guarantees in-time retraction is given by setting the above two expressions equal to one another:

$$T2_{\max} = \sqrt{\frac{2S_{P1to2rel.mech.}}{g}} - T1 + (t_{response\ min} - t_{response\ max})$$

Of course, the minimum setting which guarantees in-time release of P2 is given simply by

$$T2_{\min} = t_{response\ max}$$

The sole requirement on the duration of T3, the pulse which activates the retraction mechanism through the AC SSR, is that the width must be sufficient to ensure full retraction. Consequently,  $t_{response\ max}$  is chosen as a reasonable minimum setting.

Having addressed all of the details associated with coordinating the collision, we turn our attention to the photographic considerations. First, we must ensure that the shutter is opened by the time particle 2 reaches the top of

the camera field of view. Particle 2 will reach the field of view in an amount of time given by

$$t_{P2tofield} = T1 + t_{response\ 2\ min} + \sqrt{\frac{2(s_2 - s_{fieldtop})}{g}}$$

where

$$s_{fieldtop} = s_{coll} + \frac{y_{fieldofview}}{2}$$

and  $y_{fieldofview}$  is the vertical extent of the camera field of view. The time at which the camera shutter will open is equal to the sum of R1 and the response time associated with the external triggering mechanism of the camera. The camera response time is approximated by taking a series of photographs in which R1 is varied incrementally by 10ms and a single particle is released from the second release mechanism. The negatives are then studied to determine the lowest value of R1 which still resulted in on time opening of the shutter. This value of R1 is then subtracted from the above expression to yield the approximate response time. Once determined, this value is used to calculate R1 for future experiment geometries:

$$R1 = t_{P2tofield} - t_{cam.response}$$

For the case of the Minolta 5000i, we found that the camera response time was approximately 240ms.

Also of concern is the amount of time for which the shutter should remain open. An approximation for this value is obtained simply by subtracting the amount of time required for particle 2 to reach the top of the field of view from the time required for it to reach the bottom:

$$t_{shutter} = \sqrt{\frac{2(s_2 - s_{fieldbottom})}{g}} - \sqrt{\frac{2(s_2 - s_{fieldtop})}{g}}$$

where

$$s_{fieldbottom} = s_{coll} + \frac{y_{fieldofview}}{2} + l_2$$

Since this value represents an approximation for the minimum time open, the next larger available shutter speed is selected.

The next issues requiring attention are focus and horizontal positioning of the camera. The pre-collision distance of the particles from the camera may be found simply by recording the landing position of a single particle released from either of the two suspension mechanisms. A grid of known spacing is then placed at this position and oriented parallel to the camera plane of focus. The horizontal position of the camera is adjusted until the grid line which extends vertically upward from the landing position of the particle is in the center of the field of view. Then the aperture is opened fully, and the lens is adjusted until the grid is in focus.

Finally, an appropriate aperture setting must be determined. Since trial and error is the only known method of determining the correct f-stop in stroboscopic photography, it is necessary to shoot a roll of film at staggered aperture settings every time a significant change is made in lighting, background or particle materials.

## 2. Flat Plate

Unlike the case of binary collisions, it is a relatively simple matter to ensure that both the pre- and post-impact trajectories of a spherical particle striking a flat plate lie in the plane of focus of the camera. If the particle is in free fall prior to impact, then the camera must be positioned such that the plane of focus contains both the pre-impact trajectory and the normal to the plate surface. If the plate support is constructed so that the axis of rotational adjustment is both horizontal and perpendicular to the normal to the plate surface, then the proper camera orientation may be obtained by first adjusting the pitch of the camera until the line of focus is horizontal, then positioning the plate support such that the axis of rotation is parallel to the line of focus.

A plumb bob suspended from the particle release mechanism is useful in determining the absolute position of the plate assembly. If suspended above the surface of the plate, the bob gives an excellent indication of where the spherical particles will make contact. The bob also allows the camera position to be adjusted such that the point of contact will be near the middle, and to one side, of the field of view. The camera may be focused by fully opening the aperture and adjusting the lens until the plumb bob string is sharply defined.

After the camera and plate assembly have been positioned and oriented, it is possible to calculate the desired shutter speed and shutter trigger delay. Assuming that the spherical particle will be dropped from the lower release mechanism, R1 is given by

$$R1 = t_{P2tofield} + t_{cam.response}$$

where  $t_{P2tofield}$  is defined as it was in the case of binary collisions:

$$t_{P2tofield} = T1 + t_{respons2min} + \sqrt{\frac{2(s_2 + s_{fieldtop})}{g}}$$

An approximation for the correct shutter speed is given by twice the time required for the particle to travel from the top of the field of view to the point of contact:

$$t_{shutter} = 2 \sqrt{\frac{2(s_2 + s_{coll})}{g}} + \sqrt{\frac{2(s_2 + s_{fieldtop})}{g}}$$

Since flooding of the film by stray light is not a problem, it is recommended that a margin of safety be introduced after performing these calculations. For example, R1 may be reduced by approximately 20 milliseconds to ensure that the shutter will be open in time, and the camera shutter speed may be chosen to be one or two steps larger than that value given by the sum of  $t_{shutter}$  and the value subtracted from R1.

## B. Experiments

### 1. Binary Collisions

The appropriate timing control pulse widths have been calculated and set. The camera has been positioned and focused, the correct aperture has been determined and set, and the proper shutter speed has been selected. The release mechanisms have been aligned. Abylene tracing paper has been taped to the glass stage in the drop zone, and carbon paper has been placed smoothly over it. The strobes have been positioned, and their frequency has been set to the appropriate value. The background is in position, and sources of stray light in the laboratory have been eliminated. It is time to photograph collisions.

After loading film into the camera and checking that it has been properly advanced, the grid used to focus the camera is replaced and photographed. This grid will provide a means of relating displacements observed in following photographs to known dimensions. Next a rectangular box is set on the glass stage in front of the camera lens. The pitch of the lens is adjusted until the vertical side of the box can be placed flush against the lens opening. A line is then drawn on the abylene paper along the side of the box, providing a record of the orientation of the photo plane. The box is removed, the vacuum pump and strobes are turned on, the second release mechanism is placed in the fully forward position, and the particles are suspended. The shutter speed, aperture setting, exposure number, camera vertical position and strobe frequency are recorded on the data sheet. Then the laboratory lights are turned out, and the timing sequence is tripped. Afterwards, the lights are turned back on, the strobes turned off, the particles recovered, and their landing positions marked with the appropriate exposure number. Then the carbon paper is replaced, and the sequence is repeated until no exposures remain on the roll of film. The film is then unloaded and developed.

The film is developed as 3200 ASA as per the instructions provided with the Press Maxx developer. These instructions are summarized below:

Table 2: Recommended development times for Press Maxx developer

35mm film	E.I.	68°F 20°C	72°F 22°C	75°F 24°C
T-Max 400	400/800	5.25 min	4.5 min	4 min
	1600	8.5 min	7 min	6 min
	3200	13 min	10.5 min	9 min

After being developed, fixed, rinsed and cleaned, the film is hung to dry. The dry negatives are then cut into lengths of five exposures and placed in the sleeves of a 35mm negative file, which is labeled with the roll number and date. The negatives are then studied to determine which photographs show two pre-collision and two post-collision positions for each of the particles. Each of these exposure numbers is then found in the landing position records in order to verify that the orientation of the collision plane with respect to the photo plane can be determined. Negatives which meet both criteria are then enlarged, along with the that of the grid. Careful attention must be paid not to adjust the position of the enlarging lens while printing the set of negatives, as this would change the relationship between the displacements observed in the grid photo and those measured in the collision photos. The prints are then placed in a protective sleeve, which is also marked with the roll number and date.

## 2. Flat Plates

The flat plate experiments proceed in much the same fashion. After the preliminaries regarding positioning, alignment, timing and focus have been addressed, film is loaded into the camera and checked for proper advancement. The vacuum pump and timing control power supplies are switched on, and a

particle is suspended from the second release mechanism. The plate inclination is measured and recorded along with the shutter speed, aperture, exposure number and vertical camera position. Then the strobes are turned on, the lab lights are switched off, and the timing control circuitry is tripped. Finally, the lab lights are turned back on, the strobes switched off, and the spherical particle recovered and replaced beneath the second release mechanism. The above steps are repeated for the desired range of plate inclinations until only two exposures remain on the roll of film. Then the plate support assembly is removed, and the landing position of the particle on the drop stage is recorded. A grid of known spacing is placed before the camera in such a fashion that the grid plane coincides with the plane of focus, and the remaining two exposures are used to record the grid. Then the film is removed from the camera and developed exactly as described in the section for binary collisions. After being dried and cut, the negatives are used to make prints of the impacts, which are then scanned and analyzed.

### C. Data Analysis

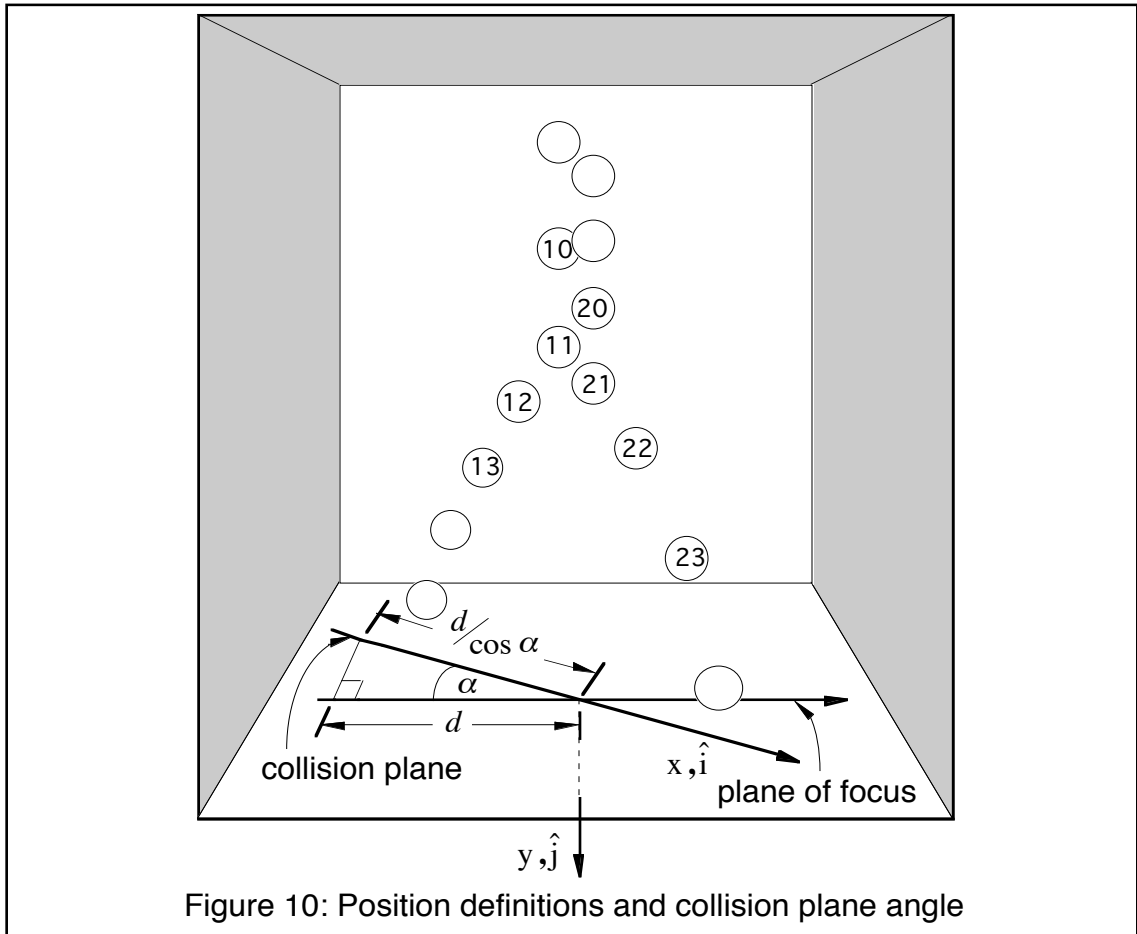
#### 1. Binary Collisions

The prints of the grid and the collisions are scanned into PICT files at a resolution of 300 DPI and then stored on data cassette. The grid file is imported into a CAD package, where the proper scaling ratio between displacements observed in the photographs and real space is determined. Knowledge of the grid spacing is used to determine the representative length of a particular line in real space, and this length is compared to the dimension returned by the CAD program. The scaling factor employed by the CAD program is then corrected by a factor of the length in real space divided by the length as reported by the program. This procedure ensures that all dimensions taken from the CAD program are representative of the actual displacements.

Next, the file of each photograph is imported into the drawing program. The two pre-collision and two post-collision positions for each particle are identified, and at each position the image observed in the photo is exactly circumscribed by a circle. After using the centers of the circles in the pre-collision positions to define vertical in the photograph, the relative positions of the circle centers are recorded on a data sheet along with the strobe frequency and relative collision plane angle,  $\angle$ , for that particular exposure. The positions of the particle centers are reported in the form  $(x_{ij}, y_{ij})$ , where  $i$  is equal to either 1 or 2 and designates the number of the particle, while  $j$  ranges from 0 to 3 and indicates the position being referenced. Particle 1 is defined to be that particle which has the greater pre-collision velocity. Position 0 is that coordinate obtained from the second to the last exposure prior to collision, position 1 corresponds to the last exposure prior to the collision, position 2 to the first exposure following the collision, and position 3 to the second post-collision exposure. These position definitions, along with the angle formed by the intersection of the photo plane and the collision plane, are illustrated in figure 10.

The entries in these data sheets are then entered in a standard format into a spreadsheet data file. A macro is used to extract the entries one at a time and substitute them into a second spreadsheet, where the information is used to determine the ballistics of the collision, and hence, the desired coefficients. When writing the spreadsheet used to analyze the information taken from the photographs, the following labels were used:

- cix - particle  $i$ , x component, pre-collision velocity of center of mass
- ciy - particle  $i$ , y component, pre-collision velocity of center of mass
- cix' - particle  $i$ , x component, post-collision velocity of center of mass



- $c_{iy}'$  - particle  $i$ ,  $y$  component, post-collision velocity of center of mass
- $c_{iypos1}$  - particle  $i$ ,  $y$  component, velocity of center of mass at position 1
- $c_{iypos2}$  - particle  $i$ ,  $y$  component, velocity of center of mass at position 2
- $t_{coll}$  - amount of time required for particles to travel from position 1 to collision, calculated using pre-collision trajectories
- $t_{collpost}$  - amount of time required for particles to travel from collision to position 2, calculated using post-collision trajectories
- $strobe_{hz}$  - frequency of strobes in cycles per second

Given the typical particle diameters and velocities of our experiments, can show that the effects of air resistance are negligible. If we define the pre-collision y component of velocity of particle i as

$$c_{iy}(t) = c_{iypos0} + at$$

then the integral of this velocity over a strobe period is equal to the vertical displacement of position 1 with respect to position 0:

$$\int_0^{\Delta t} (c_{iypos0} + at) dt = (y_{i1} - y_{i0})$$

If we neglect buoyant effects, the acceleration,  $a$ , of the spherical particle is given by

$$\begin{aligned} a &= g - \frac{F_{drag}}{m} \\ &= g - \frac{.5 \rho_{air} c_{iy}^2 C_D A}{\rho_p V} \\ &= g - \frac{3 \rho_{air} C_D c_{iy}^2}{4 \rho_p \rho_i} \end{aligned}$$

where  $C_D$  is the coefficient of drag of the sphere,  $\rho_i$  is the sphere diameter,  $\rho_{air}$  is the density of air, and  $\rho_p$  is the particle density. If we approximate the particle velocity as

$$c_{iy} = c_{iypos0} + gt$$

then

$$a = g - \frac{3 \rho_{air} C_D}{4 \rho_p \rho_i} (c_{iypos0}^2 + 2 c_{iypos0} gt + g^2 t^2)$$

and

$$\int_0^{\Delta t} (c_{iypos0} + gt - \frac{3 \rho_{air} C_D}{4 \rho_p \rho_i} (c_{iypos0}^2 t + 2 c_{iypos0} gt^2 + g^2 t^3)) dt = (y_{i1} - y_{i0})$$

Upon integrating and collecting terms involving  $c_{iypos0}$ ,

$$\begin{aligned} \left[ \frac{3 \rho_{air} C_D \Delta t^2}{8 \rho_p \rho_i} \right] c_{iypos0}^2 + \left[ \frac{\rho_{air} C_D g \Delta t^3}{2 \rho_p \rho_i} \right] c_{iypos0} + \\ \left[ \frac{g \Delta t^2}{2} - \frac{3 \rho_{air} C_D g^2 \Delta t^4}{16 \rho_p \rho_i} \right] (y_{i1} - y_{i0}) = 0 \end{aligned}$$

For the following typical values,

$$\rho_{air} = 1.2 \text{ kg / m}^3$$

$$\rho_p = 2500 \text{ kg / m}^3$$

$$g = 9.8 \text{ m / s}^2$$

$$r_i = .003 \text{ m}$$

$$C_D = .43$$

$$\Delta t = .005 \text{ s}$$

$$y_{i1} - y_{i0} = .0125 \text{ m}$$

the quadratic equation for  $c_{iypos0}$  yields

$$c_{iypos0} = 2.4763 \text{ m / s}$$

Comparing this value to that obtained assuming no air resistance

$$\int_0^{\Delta t} (c_{iypos0} + gt) dt = (y_{i1} - y_{i0})$$

$$c_{iypos0} = \frac{(y_{i1} - y_{i0})}{\Delta t} - \frac{g\Delta t}{2}$$

$$= 2.4755$$

we find an error of

$$\% \text{ error} = \frac{2.4763 - 2.4755}{2.4763} \times 100$$

$$= .032$$

Thus, the effects of air resistance are negligible. Therefore, the x components of pre- and post-collision velocities may be assumed to be constant with time and are easily calculated by dividing horizontal displacements in the collision plane by corresponding time intervals:

$$c_{ix} = \frac{(x_{i1} - x_{i0}) / \cos \theta}{\Delta t}, \quad \Delta t = \text{time between strobe}$$

flashes

$$c_{ix} = \frac{\text{strobehz} \times (x_{i1} - x_{i0})}{\cos \theta} = (1/\text{strobehz})$$

Similarly,

$$c_{ix} = \frac{\text{strobehz} \times (x_{i3} - x_{i2})}{\cos \theta}$$

It is also a simple matter to calculate the y components of velocity at particular positions. As demonstrated above,

$$c_{iypos0} = \frac{(y_{i1} - y_{i0})}{\Delta t} - \frac{g \Delta t}{2}$$

The value of  $c_{iypos1}$  follows directly

$$\begin{aligned} c_{iypos1} &= c_{iypos0} + g \Delta t \\ &= \frac{(y_{i1} - y_{i0})}{\Delta t} + \frac{g \Delta t}{2} \\ &= \text{strobeHz} * (y_{i1} - y_{i0}) + \frac{g}{2 * \text{strobeHz}} \end{aligned}$$

In a fashion analogous to the development of  $c_{iypos0}$ ,  $c_{iypos2}$  may be shown to be

$$c_{iypos2} = \text{strobeHz} * (y_{i3} - y_{i2}) - \frac{g}{2 * \text{strobeHz}}$$

Now, the above expressions can be used to calculate the y components of velocity immediately before and after the collision

$$\begin{aligned} c_{iy} &= c_{iypos1} + g * t_{coll} \\ c_{iy} &= c_{iypos2} - g * (\Delta t - t_{coll}) \end{aligned}$$

provided that an expression for  $t_{coll}$  may also be derived.

If we define the ordinates of the particle centers in the collision plane as functions of time and initial velocity

$$\begin{aligned} X_i(t) &= \frac{x_{i1}}{\cos \theta} + c_{ix} * t \\ Y_i(t) &= y_{i1} + c_{iypos1} * t + \frac{g * t^2}{2} \end{aligned}$$

then we know the particles will collide when the distance separating the two centers is equal to the sum of the radii of the spherical particles. This

condition may be expressed as

$$\sqrt{(X_2(t_{coll}) - X_1(t_{coll}))^2 + (Y_2(t_{coll}) - Y_1(t_{coll}))^2} = (r_1 + r_2)$$

Substituting for the ordinates of the particle centers and solving for  $t_{coll}$ :

$$\frac{(x_{21} - x_{11})}{\cos \theta} + (c_{2x} - c_{1x})t_{coll} + ((y_{21} - y_{11}) + (c_{2y} - c_{1y})t_{coll})^2 = (r_1 + r_2)^2$$

and after making the intermediate substitutions

$$x = (x_{21} - x_{11}) / \cos \theta$$

$$y = (y_{21} - y_{11})$$

$$V_x = (c_{2x} - c_{1x})$$

$$V_y = (c_{2y} - c_{1y})$$

we are left with

$$(x + V_x t_{coll})^2 + (y + V_y t_{coll})^2 = (r_1 + r_2)^2$$

$$(V_x^2 + V_y^2)t_{coll}^2 + 2(V_x x + V_y y)t_{coll} + (x^2 + y^2 - (r_1 + r_2)^2) = 0$$

Since we are interested in the chronologically first solution, we pick the negative root and

$$t_{coll} = \frac{-(V_x x + V_y y) - \sqrt{(V_x x + V_y y)^2 - (V_x^2 + V_y^2)(x^2 + y^2 - (r_1 + r_2)^2)}}{(V_x^2 + V_y^2)}$$

Once calculated, this value may be substituted into the expressions for the pre- and post-collision y components of velocity. In turn, these may be used with the x components to define an average value for the impulse:

$$\mathbf{J} = \frac{m_1(\mathbf{c}_1 - \mathbf{c}_1) + m_2(\mathbf{c}_2 - \mathbf{c}_2)}{2}$$

$$J_x = \frac{m_1 c_{1x} - m_2 c_{2x}}{2}$$

$$J_y = \frac{m_1(c_{1y} - c_{1y}) + m_2(c_{2y} - c_{2y})}{2}$$

Also,  $t_{coll}$  may be substituted into the expressions for the ordinates of the particle centers in order to determine the positions of the particle centers at the time of collision. As shown in Figure 2, these ordinates define a vector

extending from the center of the second particle to that of the first which forms an angle  $\gamma$  with respect to the downward vertical in the collision plane

$$\gamma_{pre} = \gamma \tan \gamma = \frac{X_2(t_{coll}) - X_1(t_{coll})}{Y_2(t_{coll}) - Y_1(t_{coll})}$$

Because it describes the orientation of the particles at the time of the collision,  $\gamma$  is a heavily weighted parameter in the calculations of the coefficients of restitution and friction. In order to determine  $\gamma$  as accurately as possible, the angle is calculated a second time using the post collision particle center trajectories. The average of the two values is then used in the coefficient calculations.

As in the previous case, we wish first to express the ordinates of the particle centers as functions of time, then solve for that value of time at which the particles will collide. The horizontal components are easily expressed as

$$X_i(t) = X_{icoll} + cix \sin \gamma t$$

where  $t$  is the time elapsed following the collision and  $X_{icoll}$  is the  $x$  ordinate of particle  $i$  at time of collision. If we set  $t = t_{collpost}$ , where  $t_{collpost}$  is equal to the time required for particle  $i$  to travel from the collision point to position 2, we know that

$$X_i(t_{collpost}) = \frac{x_{i2}}{\cos \gamma}$$

and

$$X_{icoll} = \frac{x_{i2}}{\cos \gamma} - cix \sin \gamma t_{collpost}$$

Similarly, the  $y$  ordinate expressed as a function of time is given by

$$Y_i(t) = Y_{icoll} + ciy \sin \gamma t + \frac{g t^2}{2}$$

However, we also know that

$$ciy \sin \gamma = ciy_{pos2} - g t_{collpost}$$

and

$$Y_i(t_{collpost}) = y_{i2}$$

Substituting these values and rearranging,

$$y_{i2} = Y_{icoll} + (c_{iypos2} \mp g \mp t_{collpost}) t_{collpost} + \frac{g \mp t_{collpost}^2}{2}$$

$$Y_{icoll} = y_{i2} \mp c_{iypos2} + \frac{g \mp t_{collpost}^2}{2}$$

As in the previous situation, the particles will collide when the distance separating their centers is equal to the sum of their radii:

$$(X_{2coll} \mp X_{1coll})^2 + (Y_{2coll} \mp Y_{1coll})^2 = (r_1 + r_2)^2$$

Substituting for the values of the ordinates at the collision,

$$\left( \frac{(x_{22} \mp x_{12})}{\cos \varphi} \mp (c_{2x} \mp c_{1x}) t_{collpost} \right)^2 + \left( (y_{22} \mp y_{12}) \mp (c_{2ypos2} \mp c_{1ypos2}) t_{collpost} \right)^2 = (r_1 + r_2)^2$$

and making the further substitutions

$$\Delta x = (x_{22} \mp x_{12}) / \cos \varphi$$

$$\Delta y = (y_{22} \mp y_{12})$$

$$\Delta Vx = (c_{2x} \mp c_{1x})$$

$$\Delta Vy = (c_{2y} \mp c_{1y})$$

we have

$$(\Delta x \mp \Delta Vx t_{collpost})^2 + (\Delta y \mp \Delta Vy t_{collpost})^2 = (r_1 + r_2)^2$$

$$(\Delta Vx^2 + \Delta Vy^2) t_{collpost}^2 \mp 2(\Delta x \Delta Vx + \Delta y \Delta Vy) t_{collpost} + (\Delta x^2 + \Delta y^2 \mp (r_1 + r_2)^2) = 0$$

Again, we are interested in the smallest possible solution, so we choose the negative root and

$$t_{collpost} = \frac{(\Delta x \Delta V_x + \Delta y \Delta V_y) \pm \sqrt{(\Delta x \Delta V_x + \Delta y \Delta V_y)^2 \pm (\Delta V_x^2 + \Delta V_y^2)(\Delta x^2 + \Delta y^2 \pm (r_1 + r_2)^2)}}{(\Delta V_x^2 + \Delta V_y^2)}$$

Substitution of the above value into the equations for the ordinates of the particle centers permits the definition of the second value for gamma

$$\Delta_{post} = \Delta \tan \Delta \frac{\Delta X_{2coll} \pm X_{1coll}}{\Delta Y_{2coll} \pm Y_{1coll}}$$

which can be used to define an average value for gamma

$$\Delta_{avg} = \frac{\Delta_{pre} + \Delta_{post}}{2}$$

This average value is used to express  $\mathbf{n}$ , a unit vector extending along the center line from particle 2 to particle 1, as

$$\mathbf{n} = \sin \Delta_{avg} \hat{\mathbf{i}} + \cos \Delta_{avg} \hat{\mathbf{j}}$$

The velocity and normal vector components as determined above are then substituted into the equations for the coefficients given in the section "Binary Collisions". The results are copied from the analysis spreadsheet and pasted into the original data file beside the appropriate exposure entry.

## 2. Flat Plate

Photographs of a spherical particle rebounding from a flat plate are analyzed in much the same fashion. After the photos are scanned into the CAD program, circles are drawn around the two particle positions immediately preceding the impact as well as the two following. The centers of the two pre-impact positions are used to define the vertical, and then the coordinates of all four particle centers are recorded in the form  $(x_j, y_j)$  where  $j$  ranges from 0 to 3 and indicates the position being referenced. Position 0 is that coordinate obtained from the second to the last exposure prior to impact, position 1 corresponds to the last exposure prior to the impact, position 2 to the first exposure following the impact, and position 3 to the second post-impact

exposure. These coordinates are then used to determine the pre- and post-impact velocities of the particle.

The horizontal component of the pre-impact velocity is given by

$$c_x = \frac{x_1 - x_0}{\Delta t}$$

Similarly, the post-impact horizontal component is given by

$$c_x' = \frac{x_1' - x_0}{\Delta t}$$

Calculating the vertical components requires taking into account the acceleration due to gravity between exposures. We start by calculating the vertical velocity at position 0. If we express the vertical velocity of the particle as

$$c_y(t) = c_{ypos0} + gt$$

then the vertical distance traversed in a single strobe period is given by

$$\int_0^{\Delta t} (c_{ypos0} + gt) dt = y_1 - y_0$$

making the vertical velocity at position 0 equal to

$$c_{ypos0} = \frac{y_1 - y_0}{\Delta t} - \frac{1}{2} g \Delta t$$

The vertical velocity at position 1 follows directly:

$$\begin{aligned} c_{ypos1} &= c_{ypos0} + g \Delta t \\ &= \frac{y_1 - y_0}{\Delta t} + \frac{1}{2} g \Delta t \end{aligned}$$

In an analogous fashion, we can also show that

$$c_{ypos2} = \frac{y_3 - y_2}{\Delta t} - \frac{1}{2} g \Delta t$$

These vertical velocities may now be used to pose two equations whose simultaneous solution will yield the values for  $t_{coll}$ :

$$y_{coll} = y_1 + c_{ypos1}(t_{coll}) + \frac{1}{2} g (t_{coll})^2 \quad (1)$$

$$y_{coll} = y_2 + c_{ypos2}(t_{coll}) + \frac{1}{2} g t^2 \quad (2)$$

Substituting  $y_{coll} = y_2 + c_{ypos2}(\Delta t + t_{coll})$ , the time required for the particle to move from the point of impact to position 2, into equation (2), we find

$$y_{coll} = y_2 + c_{ypos2}(\Delta t + t_{coll}) + \frac{1}{2} g (\Delta t + t_{coll})^2$$

Equating this equation with (1) and solving for  $t_{coll}$ , we are left with

$$t_{coll} = \frac{(y_1 - y_2 + cy_{pos2} - cy_{pos1} + \frac{1}{2}g\bar{t}^2)}{(cy_{pos2} - cy_{pos1} - g\bar{t})}$$

Finally, the value obtained from this expression may be substituted into the following expressions to determine the pre- and post-impact vertical components of velocity:

$$cy = cy_{pos1} + gt_{coll}$$

$$cy' = cy_{pos2} - g(\bar{t} - t_{coll})$$

The values of the vertical and horizontal velocity components are then used by the analysis spreadsheet to calculate the coefficients of normal restitution, tangential restitution and friction according to the expressions developed in the section "Impacts Between Spherical Particles and Flat Plates".

## CHAPTER 2: BINARY COLLISIONS

Binary collisions of spherical particles are assumed to occur instantaneously and to be fully described by three parameters- the coefficients of normal restitution, tangential restitution, and friction. That is, once empirically determined for a given set of particle geometries and materials, the coefficients may be used to relate uniquely the pre- and post-collision velocities. Since the coefficients succinctly summarize the effects of the many physical mechanisms involved in binary collisions, including plastic and elastic deformations, lubrication and wave propagations, they facilitate the development of velocity distribution functions for real systems involving thousands of particles assumed to interact only through binary collisions.

In this chapter, we derive relations of the pre- and post-collision velocities based on a simple model of three parameters. For consistency with existing theories, our notation follows that of Jenkins (1992).

Binary collisions are assumed to be of two types, distinguished by the behavior of the point of contact. If the point of contact slips during the collision, the interaction is said to be one of "slipping" contact, and the tangential impulse is assumed to be related to the normal impulse through Coulombic friction,

$$|\mathbf{J} \cdot \mathbf{t}| = \mu (\mathbf{J} \cdot \mathbf{n})$$

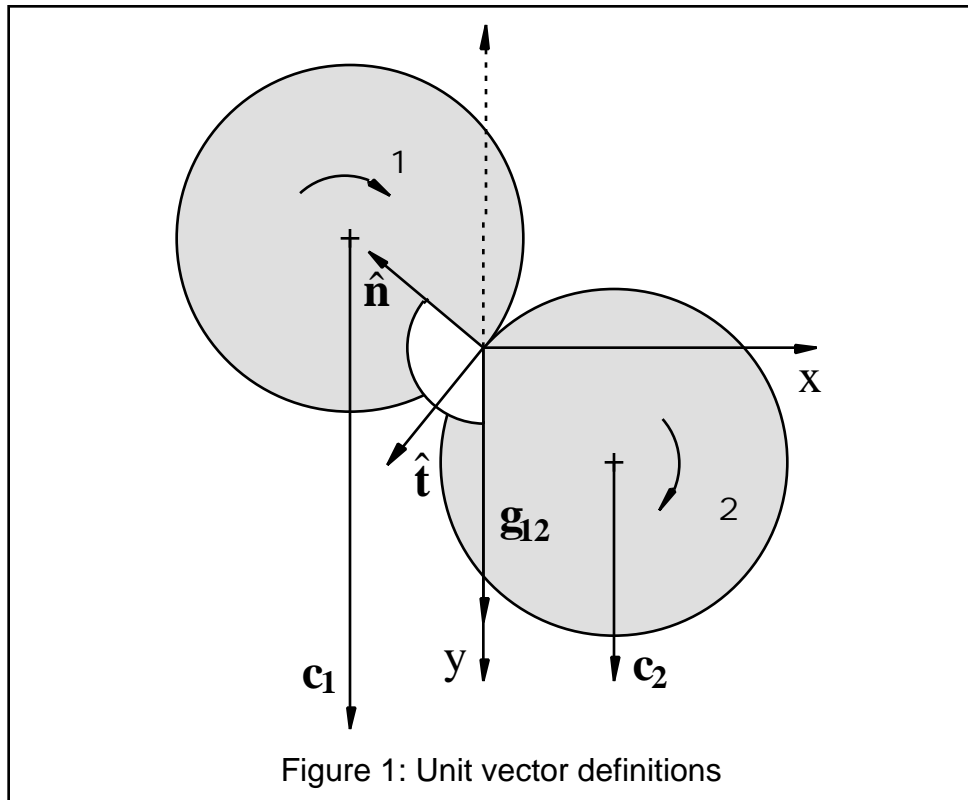
where  $\mathbf{n}$  and  $\mathbf{t}$  are the unit normal and unit tangent vectors, respectively, and  $\mu$  is the coefficient of friction. For two spherical particles in contact,  $\mathbf{n}$  is defined as

$$\mathbf{n} = \frac{\mathbf{r}_1 - \mathbf{r}_2}{|\mathbf{r}_1 - \mathbf{r}_2|}$$

where  $\mathbf{r}_1$  and  $\mathbf{r}_2$  are the positions of the particle centers, and the unit tangent vector is defined unambiguously as

$$\begin{aligned}
 \mathbf{t} &= \frac{(\mathbf{g}_{12} - (\mathbf{g}_{12} \cdot \mathbf{n})\mathbf{n})}{\sqrt{|\mathbf{g}_{12}|^2 - (\mathbf{g}_{12} \cdot \mathbf{n})^2}} \\
 &= -n_y \hat{\mathbf{i}} + n_x \hat{\mathbf{j}} \\
 &= -\cos \hat{\mathbf{i}} - \sin \hat{\mathbf{j}}
 \end{aligned}$$

where  $\mathbf{g}_{12}$  is the pre-collision relative velocity of the points of contact,  $\theta$  is the positive clockwise angle measured from  $\mathbf{g}_{12}$  to  $\mathbf{n}$ , and  $\hat{\mathbf{i}}$  and  $\hat{\mathbf{j}}$  are orthogonal unit vectors which span the collision plane. The vectors  $\hat{\mathbf{i}}$  and  $\hat{\mathbf{j}}$  lie such that  $\hat{\mathbf{j}}$  is parallel to the downward vertical and  $\hat{\mathbf{i}} \times \hat{\mathbf{j}}$  is in the direction of the line of sight.



Collisions in which the point of contact remains locked are described as rolling or "sticking" collisions. In such instances, it is assumed that the tangential components of the pre-and post-collision relative velocities are related by a constant factor:

$$\mathbf{g}_{12} \cdot \mathbf{t} = -\epsilon_0 (\mathbf{g}_{12} \cdot \mathbf{t})$$

where  $e_0$  is the coefficient of tangential restitution. In either case, it is assumed that the post-collision normal component of the relative velocity is related to the pre-collision normal component by the coefficient of normal restitution,  $e$ :

$$\mathbf{g}_{12} \cdot \mathbf{n} = -e(\mathbf{g}_{12} \cdot \mathbf{n})$$

These definitions may be used to determine the values of the coefficients provided that the orientation of  $\mathbf{n}$ , type of collision, and values of the pre- and post-collision relative velocities may be determined.

If the particles are released with no initial angular velocity, the pre-collision relative velocity of the contact point is given simply by

$$\mathbf{g}_{12} = \mathbf{c}_1 - \mathbf{c}_2$$

where  $\mathbf{c}_i$  is the pre-collision velocity of the center of mass for particle  $i$ . If we assume further that the particles are spheres of diameter  $d_i$ , then the post-collision relative velocity at the point of contact is given by

$$\begin{aligned} \mathbf{g}_{12} &= \mathbf{g}_1 - \mathbf{g}_2 \\ &= (\mathbf{c}_1 - \mathbf{c}_2) + \frac{\mathbf{n}}{2} \times (\boldsymbol{\omega}_1 d_1 + \boldsymbol{\omega}_2 d_2) \end{aligned}$$

where

$$\begin{aligned} \mathbf{g}_1 &= \mathbf{c}_1 + \frac{1}{2} \mathbf{n} \times \boldsymbol{\omega}_1 \\ \mathbf{g}_2 &= \mathbf{c}_2 - \frac{2}{2} \mathbf{n} \times \boldsymbol{\omega}_2 \end{aligned}$$

The angular velocity terms in the above expressions may be expressed in terms of pre- and post-collision translational velocities using the principle of conservation of angular momentum. The angular momentum of a sphere about a point on its surface is given by

$$\mathbf{H} = I_{cm} \boldsymbol{\omega} + \mathbf{r} \times m\dot{\mathbf{r}}$$

where  $\mathbf{r}$  extends from the point of contact to the center of the sphere. Since all interactive forces in a binary collision act through the point of contact, the angular momentum of each particle about the point of contact is conserved.

Thus, the angular momentum conservation equations for our system may be expressed as

$$I_{1cm} \omega_1 + \frac{1}{2} \mathbf{n} \times m_1 \mathbf{c}_1 = I_{1cm} \omega_1 + \frac{1}{2} \mathbf{n} \times m_1 \mathbf{c}_1$$

$$I_{2cm} \omega_2 - \frac{2}{2} \mathbf{n} \times m_2 \mathbf{c}_2 = I_{2cm} \omega_2 - \frac{2}{2} \mathbf{n} \times m_2 \mathbf{c}_2$$

In the case that the pre-collision angular velocities are zero, these equations imply that

$$\left( \omega_1 + \omega_2 \right) = -\frac{1}{2} \left( \frac{1}{I_{1cm}} + \frac{2}{I_{2cm}} \right) \mathbf{n} \times \mathbf{J}$$

where  $\mathbf{J}$  is the impulse, given by

$$\mathbf{J} = m_1 (\mathbf{c}_1 - \mathbf{c}_1) = m_2 (\mathbf{c}_2 - \mathbf{c}_2)$$

Substituting into the expression for the post-collision relative velocity we find

$$\mathbf{g}_{12} = (\mathbf{c}_1 - \mathbf{c}_2) - \frac{1}{4} \left( \frac{1}{I_{1cm}} + \frac{2}{I_{2cm}} \right) ((\mathbf{n} \cdot \mathbf{J}) \mathbf{n} - \mathbf{J})$$

and if we express the moments of inertia of the spheres in terms of the masses and diameters of the particles,

$$I_{icm} = \frac{m_i d_i^2}{10}$$

then

$$\mathbf{g}_{12} = (\mathbf{c}_1 - \mathbf{c}_2) - \frac{5}{2} \frac{m_1 + m_2}{m_1 m_2} ((\mathbf{n} \cdot \mathbf{J}) \mathbf{n} - \mathbf{J})$$

Substitution of the above expressions for the pre- and post-collision relative velocities into the definitions of the coefficients of normal restitution, tangential restitution and friction yields expressions involving only translational velocities, particle masses, and components of  $\mathbf{n}$ . For example, the coefficient of normal restitution becomes

$$e = \frac{-\mathbf{g}_{12} \cdot \mathbf{n}}{\mathbf{g}_{12} \cdot \mathbf{n}}$$

$$= \frac{-(\mathbf{c}_1 - \mathbf{c}_2) \cdot \mathbf{n}}{(\mathbf{c}_1 - \mathbf{c}_2) \cdot \mathbf{n}}$$

and if we assume that the pre-collision horizontal components of velocity are zero, we may express  $e$  in component form as

$$\begin{aligned} e &= \frac{-(c_{1x} - c_{2x})n_x - (c_{1y} - c_{2y})n_y}{(c_{1y} - c_{2y})n_y} \\ &= \frac{(c_{1x} - c_{2x})}{(c_{1y} - c_{2y})} \tan \theta - \frac{(c_{1y} - c_{2y})}{(c_{1y} - c_{2y})} \end{aligned}$$

Similarly, the coefficient of tangential restitution becomes

$$\begin{aligned} e_0 &= \frac{-\mathbf{g}_{12} \cdot \mathbf{t}}{\mathbf{g}_{12} \cdot \mathbf{t}} \\ &= \frac{-(\mathbf{c}_1 - \mathbf{c}_2) \cdot \mathbf{t} + \frac{5}{2} \frac{m_1 + m_2}{m_1 m_2} \mathbf{J} \cdot \mathbf{t}}{\mathbf{g}_{12} \cdot \mathbf{t}} \\ &= \frac{[(c_{1x} - c_{2x})n_y - (c_{1y} - c_{2y})n_x] + \frac{5}{2} \frac{m_1 + m_2}{m_1 m_2} (J_x n_y - J_y n_x)}{(c_{1y} - c_{2y})n_x} \\ &= \frac{-(c_{1x} - c_{2x})}{(c_{1y} - c_{2y})} \cot \theta - \frac{(c_{1y} - c_{2y})}{(c_{1y} - c_{2y})} + \frac{5}{2} \frac{m_1 + m_2}{m_1 m_2} \frac{(-J_x \cot \theta - J_y)}{(c_{1y} - c_{2y})} \end{aligned}$$

and finally, the coefficient of friction takes the form

$$\begin{aligned} \mu &= \frac{|\mathbf{J} \cdot \mathbf{t}|}{\mathbf{J} \cdot \mathbf{n}} \\ &= \frac{|-J_x n_y + J_y n_x|}{J_x n_x + J_y n_y} \\ &= \frac{|J_x + J_y \tan \theta|}{J_y - J_x \tan \theta} \text{sign}[n_y] \end{aligned}$$

The above expressions may be used to determine the coefficients for a particular collision directly. However, since it is not known *a priori* if the collision is one of slipping or sticking contact, it is not immediately known which of the tangential restitution and friction coefficients is meaningful. The distinction is made by plotting the non-dimensional post-collision tangential component of relative velocity, defined as

$$e_2 = \frac{\mathbf{g}_{12} \cdot \mathbf{t}}{\mathbf{g}_{12} \cdot \mathbf{n}}$$

$$\begin{aligned}
& \frac{(\mathbf{c}_1 - \mathbf{c}_2) \cdot \mathbf{t} + \frac{5}{2} \frac{m_1 + m_2}{m_1 m_2} \mathbf{J} \cdot \mathbf{t}}{(\mathbf{g}_{12} \cdot \mathbf{n})} \\
&= \frac{-(c_{1x} - c_{2x})n_y + (c_{1y} - c_{2y})n_x - \frac{5}{2} \frac{m_1 + m_2}{m_1 m_2} (J_x n_y - J_y n_x)}{(c_{1y} - c_{2y})n_y} \\
&= \frac{-(c_{1x} - c_{2x}) - (c_{1y} - c_{2y}) \tan \theta - \frac{5}{2} \frac{m_1 + m_2}{m_1 m_2} (J_x + J_y \tan \theta)}{(c_{1y} - c_{2y})}
\end{aligned}$$

versus the pre-collision tangential component of relative velocity

$$\begin{aligned}
v_1 &= \frac{\mathbf{g}_{12} \cdot \mathbf{t}}{\mathbf{g}_{12} \cdot \mathbf{n}} \\
&= -\tan \theta
\end{aligned}$$

In the case of sticking contact, we expect  $v_2$  to vary with  $v_1$  as

$$\begin{aligned}
v_2 &= \frac{-v_1 (\mathbf{g}_{12} \cdot \mathbf{t})}{\mathbf{g}_{12} \cdot \mathbf{n}} \\
&= -v_1
\end{aligned}$$

and in the region of sliding contact, we use the definition of the friction coefficient as well as the expression derived earlier for  $\mathbf{g}_{12}$  to find that

$$\begin{aligned}
v_2 &= \frac{(\mathbf{c}_1 - \mathbf{c}_2) \cdot \mathbf{t} - \frac{5}{2} \frac{m_1 + m_2}{m_1 m_2} ((\mathbf{n} \cdot \mathbf{J})\mathbf{n} - \mathbf{J}) \cdot \mathbf{t}}{\mathbf{g}_{12} \cdot \mathbf{n}} \\
&= \frac{\frac{\mathbf{J}}{m_1} + \mathbf{c}_1 - \mathbf{c}_2 - \frac{\mathbf{J}}{m_2} + \frac{5}{2} \frac{m_1 + m_2}{m_1 m_2} \mathbf{J} \cdot \mathbf{t}}{\mathbf{g}_{12} \cdot \mathbf{n}} \\
&= \frac{(\mathbf{g}_{12} \cdot \mathbf{t}) + \frac{7}{2} \frac{m_1 + m_2}{m_1 m_2} \mathbf{J} \cdot \mathbf{t}}{\mathbf{g}_{12} \cdot \mathbf{n}}
\end{aligned}$$

$$\begin{aligned}
&= \frac{7\mu}{2} \frac{m_1 + m_2}{m_1 m_2} (\mathbf{J} \cdot \mathbf{n}) \text{sign}(\mathbf{J} \cdot \mathbf{t}) \\
&= \frac{7\mu}{2} \frac{(\mathbf{c}_2 - \mathbf{c}_2 + \mathbf{c}_1 - \mathbf{c}_1) \cdot \mathbf{n}}{\mathbf{g}_{12} \cdot \mathbf{n}} \text{sign}(\mathbf{J} \cdot \mathbf{t}) \\
&= \frac{7\mu}{2} (1 + e) \text{sign}(\mathbf{g}_{12} \cdot \mathbf{t})
\end{aligned}$$

Thus, a plot of  $\dot{x}_2$  over a sufficient range of  $x_1$  will yield two linear regimes defining the domains of sticking and sliding contact.  $x_0$  and  $\mu$  may be determined either from the slopes and intercepts produced by regression analyses of the two regimes, or from the values produced by the coefficient definition appropriate to each regime.

## CHAPTER 3: FLAT PLATE IMPACTS

The post-impact velocity of a solid sphere rebounding from a flat plate is related to the pre-impact velocity through a number of physical mechanisms and system parameters. Fluid lubrication, material elasticities, and wave propagations all factor into the way energy is exchanged and forces are directed at the point of contact. As in the case of binary collisions, it is assumed that the empirically determined coefficients of normal restitution, tangential restitution and friction may be used to describe fully the effects of these complex physical mechanisms for a given system geometry and composition:

$$\mathbf{g}_1 \cdot \mathbf{n} = e(\mathbf{g}_{12} \cdot \mathbf{n})$$

$$\mathbf{g}_1 \cdot \mathbf{t} = \mu_0 (\mathbf{g}_{12} \cdot \mathbf{t})$$

$$|\mathbf{J} \cdot \mathbf{t}| = \mu (\mathbf{J} \cdot \mathbf{n})$$

Though defined in exactly the same way, the coefficients for an impact with a flat plate differ from those for a binary collision in that the post-collision relative velocity is given by

$$\begin{aligned} \mathbf{g}_1 &= (\mathbf{c}_1 - \mathbf{c}_2) - \frac{5}{2} \frac{m_1 + m_2}{m_1 m_2} ((\mathbf{n} \cdot \mathbf{J}) \mathbf{n} - \mathbf{J}) \\ &= \mathbf{c}_1 - \frac{5}{2 m_1} ((\mathbf{n} \cdot \mathbf{J}) \mathbf{n} - \mathbf{J}) \end{aligned}$$

since the mass of the plate is assumed to be infinite and its post-impact translational velocity is zero. Also,  $\mathbf{n}$  is redefined to be the unit normal to the plate surface. Substitution of these new values into the coefficient definitions and non-dimensional tangential components of relative velocity results in the following expressions for impact of a spherical particle with a flat plate:

$$\begin{aligned} e &= \frac{c_{1x}}{c_{1y}} \tan \theta - \frac{c_{2x}}{c_{2y}} \\ \mu_0 &= \frac{c_{1x}}{c_{1y}} \cot \theta - \frac{c_{2x}}{c_{2y}} + \frac{5}{2 m_1} \frac{J_x \cot \theta - J_y}{c_{1y}} \end{aligned}$$

$$\theta = \frac{|J_y \tan \theta + J_x|}{J_y - J_x \tan \theta} \text{sign}[n_y]$$

and

$$\theta_1 = \theta \tan \theta$$

$$\theta_2 = \frac{c_1 \theta - c_2 \tan \theta}{c_{1y}} \frac{5}{2m_1} (J_x + J_y \tan \theta)$$

Since the coefficients empirically describe the behavior of the system without regard to material properties or system geometry, their validity is restricted to that system for which they are calculated. In the case of binary collisions, a system could be fully described simply by reporting only the particle diameters, compositions, and finishes. However, the behavior of a spherical particle/flat plate system is also dependent upon the plate thickness, material, and support geometry, as demonstrated by Sondergaard, Chaney and Brennen (1990). In particular, the authors observed that the coefficient of normal restitution varies with displacement from the plate supports up to a critical distance approximated by

$$s_{crit} = \frac{c T_c}{2}$$

where  $c$  is the speed of the shear waves generated in the plate by the impact and  $T_c$  is the Hertzian contact time. Assuming a Poisson's ratio of .3 for the plate material, the shear wave speed is given by

$$c = .62 \sqrt{\frac{E_p}{\rho_p}}$$

where  $\rho_p$  and  $E_p$  are the density and modulus of elasticity of the plate, respectively. The Hertzian contact time for a sphere on a semi-infinite block is equal to

$$T_c = 5.08a \left[ (1 - \nu_s^2) + (1 - \nu_p^2) E_s / E_p \right]^{2/5} \frac{\rho_s}{E_s}^{2/5} (\mathbf{g}_{12} \cdot \mathbf{n})^{1/5}$$

where  $\nu_s$  and  $\nu_p$  are Poisson's ratios for the sphere and plate, respectively, and  $a$  is the sphere radius. Thus, if the coefficients calculated for a spherical particle/flat plate system are to be independent of position, care must be taken to study only those impacts which occur at a minimum distance  $s_{crit}$  away from the nearest plate support.

$$s_{crit} = 1.57a \sqrt{\frac{E_p}{E_s}} \left[ (1 - \nu_s^2) + (1 - \nu_p^2) E_s / E_p \right]^{2/5} \left( \frac{E_p}{E_s} \right)^{2/5} (c_{1y} \cos \theta)^{1/5}$$

## CHAPTER 5: RESULTS

The results of the binary collision and flat plate experiments are summarized in the following table:

Table 3: Collision coefficients

	3mm glass binary collision	3mm glass on flat Al plate	6mm acetate binary collision	6mm acetate on flat Al plate
e	.97 ±.01	.831 ±.009	.87 ±.02	.891 ±.003
$\beta_0$	.44 ±.07	.34 ±.04	.43 ±.06	.39 ±.07
$\mu$	.092 ±.006	.125 ±.007	.25 ±.02	.208 ±.007

The coefficient of normal restitution,  $e$ , is found simply by averaging the values obtained from individual collisions in both the sticking contact and sliding contact regions. The coefficients of tangential restitution and friction,  $\beta_0$  and  $\mu$  respectively, are calculated by averaging the values calculated individually in each of the appropriate regimes. The extents of the sticking contact and sliding contact domains are determined by plotting  $\Delta_2$  versus  $\Delta_1$ . The value of  $\Delta_1$  at which the two regimes intersect is visually estimated, and then the data field is bisected by this value. A line passing through the origin is fit by least squares to the data field for sticking collisions, and a line of slope 1 is fit by least squares to the sliding contact data. The intersection of these two lines is then used as the new approximation for that value of  $\Delta_1$  which bisects the original data field into the sliding contact and sticking contact domains. This iterative process is repeated until the intersection of the fitted lines generates the same data subsets used to fit the lines.

Each element in a data set is evaluated according to Chauvenet's criterion, as given by Holman (1978). The criterion states that a reading may be

rejected if the probability of obtaining the particular deviation from the mean is less than  $1/2n$ , where  $n$  is the number of elements in a normally distributed set. For  $n < 50$ , the maximum acceptable deviation of an observed value from the mean is well approximated by

$$d_{\max} = \sigma \left[ .74682 + .61967 \ln(n) - .039511 \ln(n)^2 \right]$$

where  $\sigma$  is the sample standard deviation. Data points which differ from the mean by a value greater than  $d_{\max}$  are rejected, and the sample mean is recalculated. Chauvenet's criterion is never applied more than once to the same data set. The results of this criterion are given in the following table:

Table 4: Chauvenet's criterion results

	3mm glass binary collision		6mm acetate binary collision		3mm glass on flat Al plate		6mm acetate on flat Al plate	
	n	rejected	n	rejected	n	rejected	n	rejected
e	24	0	38	2	19	0	23	1
$\beta_0$	13	1	24	0	10	2	15	1
$\mu$	11	0	14	1	9	0	8	0

The error associated with the average value of each coefficient is then calculated using Student's t distribution. The test statistic is defined as

$$t = \frac{\bar{x} - \mu}{\sigma_{n-1} / \sqrt{n}}$$

where  $\bar{x}$  is the sample mean,  $\mu$  is the population mean,  $\sigma_{n-1}$  is the sample standard deviation, and  $n$  is the sample size. The value of  $t$  is chosen for  $(n-2)$  degrees of freedom such that the likelihood of the absolute value of the test statistic being greater than or equal to  $t$  is equal to 20%. This implies there is an 80% chance that

$$t_{n,2,2} > \frac{|\bar{x} - \mu|}{\frac{s}{\sqrt{n}}}$$

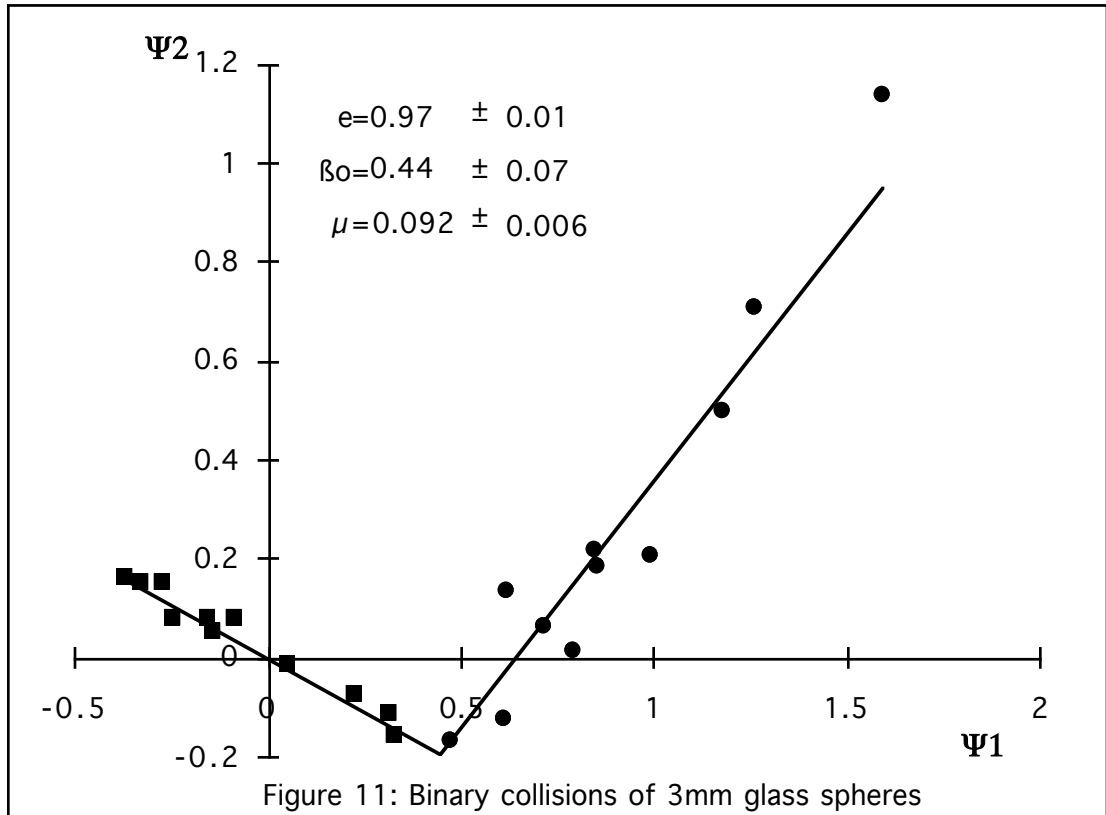
$$|\bar{x} - \mu| < \frac{s t_{n,2,2}}{\sqrt{n}}$$

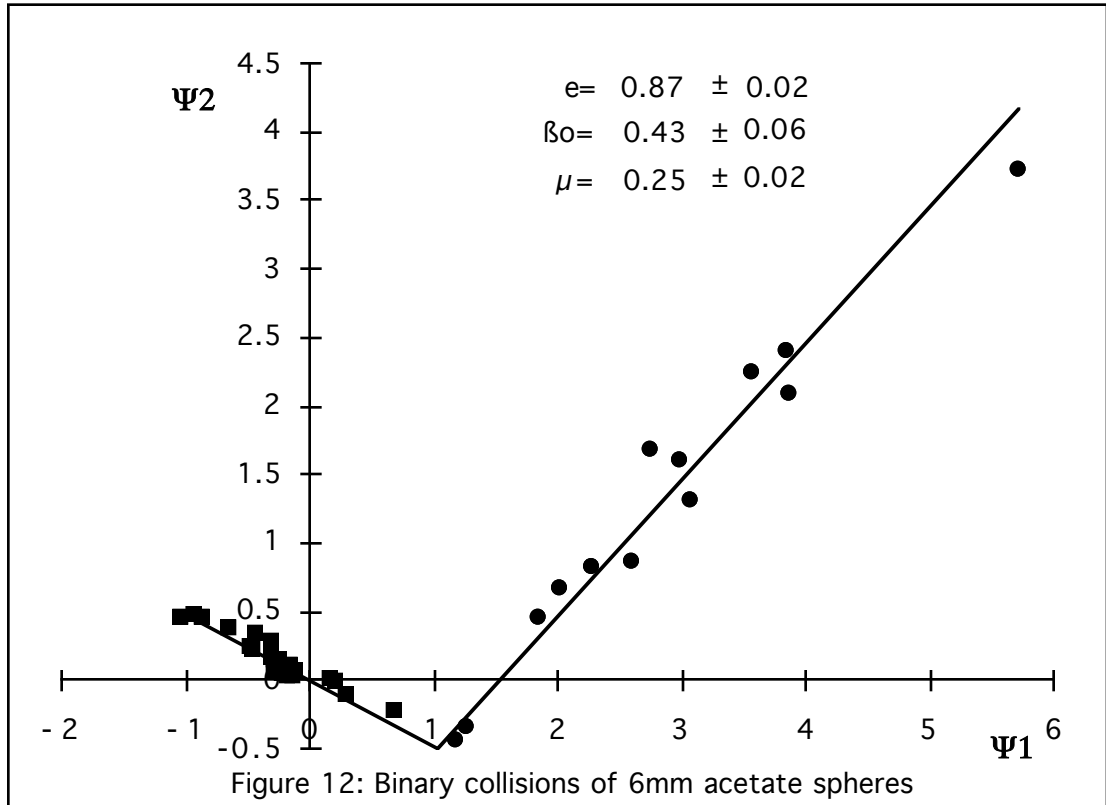
or stated another way, we are 80% confident that the population mean lies in the following interval:

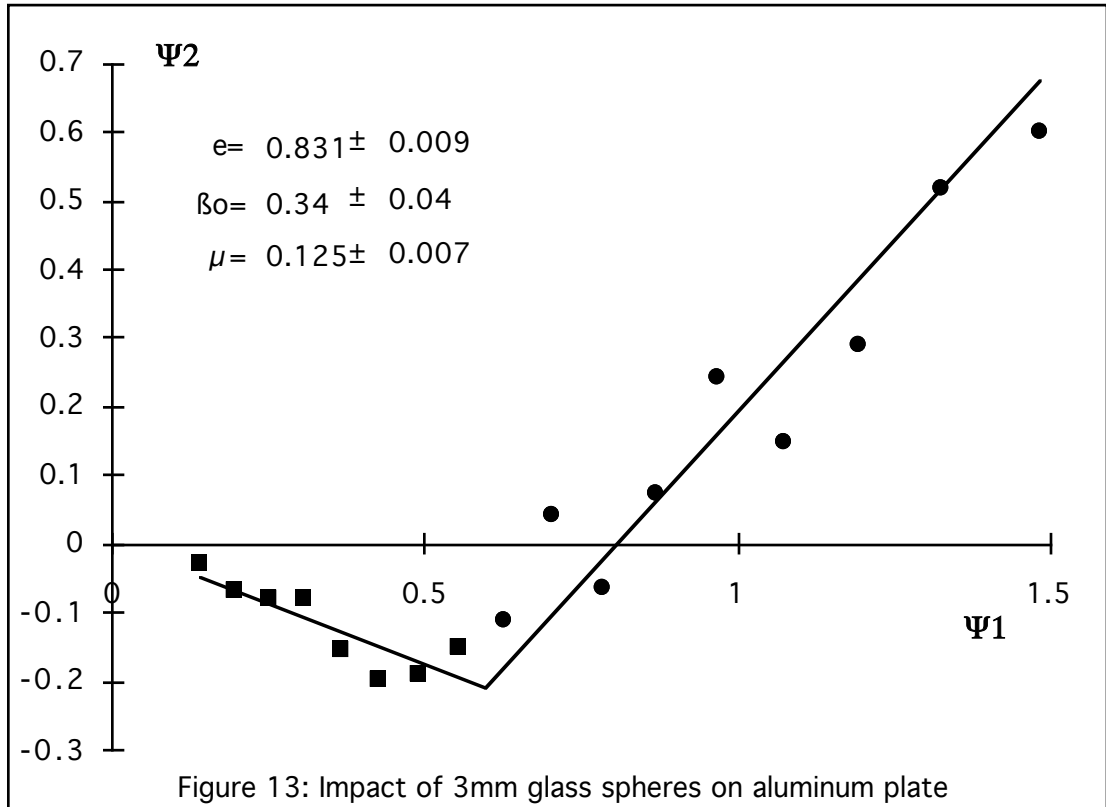
$$\mu = \bar{x} \pm \frac{s t_{n,2,2}}{\sqrt{n}}$$

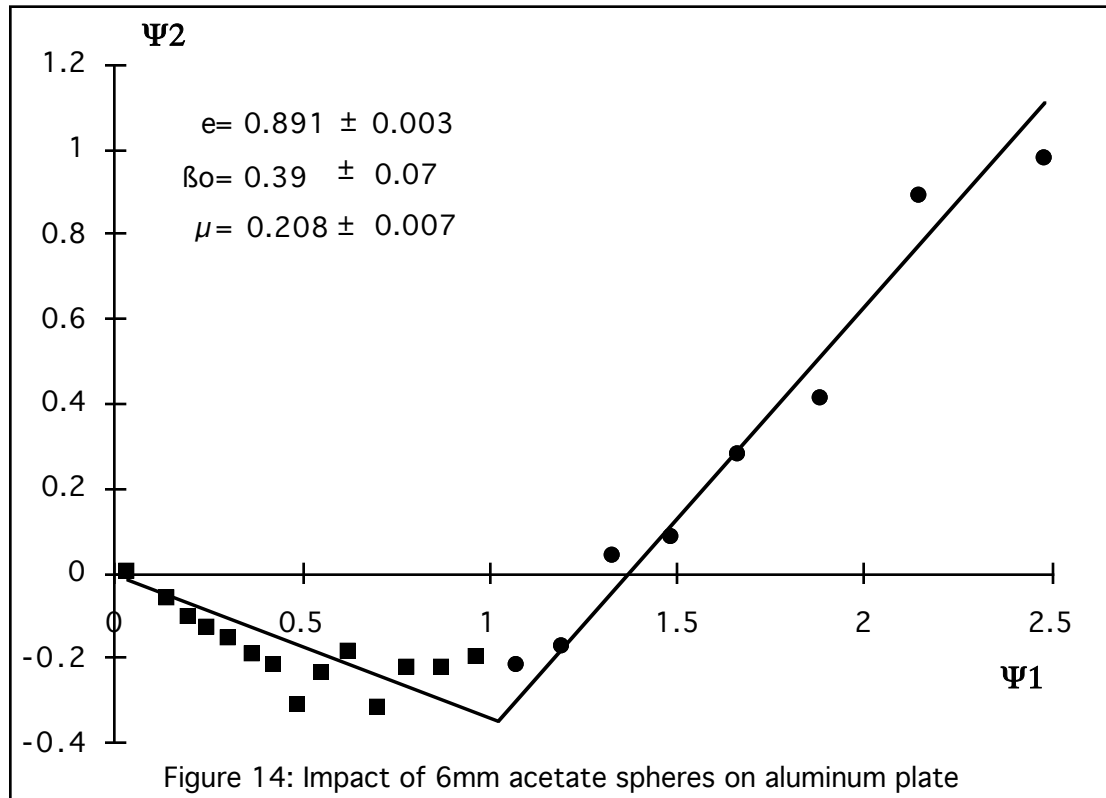
The plots of  $\mu_2$  versus  $\mu_1$  for 3mm glass spheres and 6mm acetate spheres in binary collisions follow in figures 11 and 12. It is clear in both cases that two well-defined linear regimes exist, demonstrating that the particle collision coefficient definitions presented in the section "Binary Collisions" adequately summarize the effects of the physical mechanisms relating the pre- and post-collision relative velocities of the points of contact. Foerster and Louge (1993) show that the same data also follow closely the model of Maw, Barber and Fawcett (1981). Though the diameters, elastic moduli and densities of the glass and acetate particles all differ by factors of approximately two, the coefficients of normal and tangential restitution are remarkably similar. The only coefficient presenting a striking difference is that of friction, probably suggesting a difference in surface roughness of the two types of particles. The coefficient of normal restitution obtained for acetate spheres,  $e=.87\pm.02$ , compares favorably with the value of  $e=.84\pm.01$  presented by Drake (1991).

In the plots of  $\mu_2$  versus  $\mu_1$  for impacts of 3mm glass and 6mm acetate spheres on a thick aluminum plate (figures 13 and 14), we again observe the two linear regions corresponding to sliding and sticking contact. In the case of glass spheres, we see that the coefficients of normal and tangential restitution are significantly lower than the corresponding values observed in binary collisions. However, the same coefficients for acetate spheres are nearly









identical to those observed in binary collisions of acetate spheres. The coefficient of friction observed for glass spheres in flat plate collisions is approximately 35% higher than that seen in binary collisions of the same particles, while  $\mu$  for flat plate collisions is found to be nearly 17% lower than that for binary collisions in the case of acetate spheres. The observed value of  $\mu = 0.208 \pm 0.007$  for 6mm acetate spheres on a thick aluminum plate is very similar to the value of  $\mu = 0.21 \pm 0.07$  reported by Drake (1991) for 6mm acetate spheres on a glass plate.

Plots of the coefficient of normal restitution versus the normal component of the relative velocity of the point of contact (not shown) offer no evidence of a relationship between  $e$  and  $\mathbf{g}_{12} \cdot \mathbf{n}$ . It should be noted, however, that the ranges of  $\mathbf{g}_{12} \cdot \mathbf{n}$  studied in the binary collision and flat plate experiments are quite small. In the case of binary collisions, values of  $\mathbf{g}_{12} \cdot \mathbf{n}$  range from -1.26 m/s to -

.65 m/s, while the same values for flat plate impacts lie in the interval -1.78 m/s to -1.17 m/s. Similarly, plots of the coefficient of tangential restitution versus the tangential component of the relative velocity of the point of contact indicate no discernible relationship between  $\beta_0$  and  $\mathbf{g}_{12} \cdot \mathbf{t}$  in the ranges of  $.14 \text{ m/s} < |\mathbf{g}_{12} \cdot \mathbf{t}| < 1.0 \text{ m/s}$  for binary collisions and  $.06 \text{ m/s} < |\mathbf{g}_{12} \cdot \mathbf{t}| < 1.5 \text{ m/s}$  for impacts with flat plates.

Analysis of the photographs themselves reveals that the trajectories of the particles immediately prior to a binary collision are not exactly parallel. In fact, they appear to converge with an angle of separation varying around .3 degrees. The converging trajectories probably reflect the effect of the turbulent wake of the second particle on the first. Since the angle of convergence is consistently small, the vertical direction is simply approximated as the trajectory of one particle or the other, and horizontal and vertical components of pre- and post-collision velocities are expressed accordingly.

## CHAPTER 6: CONCLUSIONS

The results demonstrate conclusively that the relationships

$$\begin{aligned} \bar{\mu}_2 &= \bar{\mu}_0 \bar{\mu}_1 \\ \bar{\mu}_2 &= \bar{\mu}_1 + \frac{7\bar{\mu}}{2}(1+e)\text{sign}(\mathbf{g}_{12} \cdot \mathbf{t}) \end{aligned}$$

predicted by the collision coefficient definitions

$$\begin{aligned} \mathbf{g}_2 \cdot \mathbf{n} &= e(\mathbf{g}_1 \cdot \mathbf{n}) \\ \mathbf{g}_2 \cdot \mathbf{t} &= \bar{\mu}_0(\mathbf{g}_1 \cdot \mathbf{t}) \\ \mathbf{J} \cdot \mathbf{t} &= \bar{\mu}(\mathbf{J} \cdot \mathbf{n}) \end{aligned}$$

constitute a valid model for spherical particles involved in both binary collisions and impacts with flat plates. Thus, the collision coefficients may be used to uniquely relate the pre- and post-impact relative velocities of the points of contact for spherical particles involved in binary and flat plate collisions. In order to predict the impulse and collision velocities, it is reasonable to assume that the collisions occur instantaneously and that there exist two types of contact differentiated by the sticking or sliding behavior of the point of contact at the time of the collision.

The facility used to collect the data has proven itself effective, but the method of data collection could be significantly improved in two ways. First, the conventional camera and film could be replaced by a fully digital camera, eliminating all steps involved in developing the film, printing the photographs, and scanning the prints. A digital camera would also facilitate set-up of experiments by introducing an almost immediate feedback loop. Rather than taking the time to calculate solenoid response times and air drag effects for each new set of particles, an experimentalist would merely approximate the required timing control circuitry pulse widths. Then photos would be taken and viewed on a computer screen, and the pulse widths would be readjusted as necessary.

Kodak currently offers a 1524x1012 line digital camera having a light sensitivity comparable to 800 ISO film. The unit, called a DCS-200, costs approximately \$9100 and has proven itself extremely effective in on-site demonstrations. The second major improvement could be made in the analysis of the digitized images. Currently, analysis involves loading each file into a CAD program, manually drawing circles around each image of the spherical particles, reading and recording the positions of the circle centers, and entering the particle center positions in a data file. Much of this effort would be curtailed if an image analysis routine were written to open a digitized image file, locate the particle centers, and use the data to calculate the parameters  $\bar{\rho}_1$ ,  $\bar{\rho}_2$ ,  $e$ ,  $\bar{\rho}_0$  and  $\mu$ .

## REFERENCES

Craig, K.C., Buckholz, R. and Domoto, G., 1986, "An experimental study of the rapid flow of dry cohesionless metal powders," *Trans. ASME E: J. Appl. Mech.*, Vol.53, pp. 935-952

Drake, T. G., 1991, "Granular flow: physical experiments and their implications for microstructural theories," *Journal of Fluid Mechanics*, Vol. 225, pp. 121-152.

Foerster, S., and Louge, M., 1993, "Measurements of the particle collision properties of small spheres," *Physics of Fluids A*, in review.

Holman, J.P., 1978, Experimental Methods for Engineers, McGraw-Hill Book Company, p. 65

Jenkins, J.T., 1992, "Boundary conditions for rapid granular flow: flat, frictional walls," *ASME J. of Applied Mechanics*, Vol.59, pp. 120-127

Johnson, P.C., Nott, P. and Jackson, R., 1990, "Frictional-collisional equations of motion for particulate flow and their applications to chutes," *Journal of Fluid Mechanics*, Vol. 210, pp. 501-535

Maw, N., Barber, J.R., and Fawcett, J.N., 1981, "The role of elastic tangential compliance in oblique impact," *ASME J. of Lubrication Technology*, Vol. 103, pp. 74-80

Sondergaard, R., Chaney, K., and Brennen, C.E., 1990, "Measurements of solid spheres bouncing off flat plates," *ASME J. of Applied Mechanics*, Vol. 57, pp. 694-699

Walton, O. R., 1988, "Granular Solids Flow Project, Quarterly Report, January-March 1988, UCID-20297-88-1," Lawrence Livermore National Laboratory.